Monthly Notices
of the
ROYAL ASTRONOMICAL SOCIETY

Mon. Not. R. Astron. Soc. **426,** 23–39 (2012) doi:10.1111/j.1365-2966.2012.21140.x

Molecular line contamination in the SCUBA-2 450 and 850 μm continuum data

E. Drabek,[1⋆] J. Hatchell,[1] P. Friberg,[2] J. Richer,[3,4] S. Graves,[3,4] J. V. Buckle,[3,4] D. Nutter,[5] D. Johnstone[6,7] and J. Di Francesco[6,7]

[1]*School of Physics, University of Exeter, Stocker Road, Exeter EX4 4QL*
[2]*Joint Astronomy Centre, 660 North A'ohoku Place, Hilo, HI 96720, USA*
[3]*Astrophysics Group, Cavendish Laboratory, J J Thomson Avenue, Cambridge CB3 0HE*
[4]*Kavli Institute for Cosmology, Cambridge, Madingley Road, Cambridge CB3 0HA*
[5]*School of Physics & Astronomy, Cardiff University, 5 The Parade, Cardiff CF24 3AA*
[6]*National Research Council Canada, Herzberg Institute of Astrophysics, 5071 West Saanich Road, Victoria, BC V9E 2E7, Canada*
[7]*Department of Physics & Astronomy, University of Victoria, 3800 Finnerty Road, Victoria, BC V8P 5C2, Canada*

Accepted 2012 April 19. Received 2012 April 18; in original form 2012 March 16

ABSTRACT

Observations of the dust emission using millimetre/submillimetre bolometer arrays can be contaminated by molecular line flux, such as flux from ^{12}CO. As the brightest molecular line in the submillimetre, it is important to quantify the contribution of CO flux to the dust continuum bands. Conversion factors were used to convert molecular line integrated intensities to flux detected by bolometer arrays in mJy beam^{-1}. These factors were calculated for ^{12}CO line integrated intensities to the SCUBA-2 850 and 450 μm bands. The conversion factors were then applied to HARP ^{12}CO 3–2 maps of NGC 1333 in the Perseus complex and NGC 2071 and NGC 2024 in the Orion B molecular cloud complex to quantify the respective ^{12}CO flux contribution to the 850 μm dust continuum emission. Sources with high molecular line contamination were analysed in further detail for molecular outflows and heating by nearby stars to determine the cause of the ^{12}CO contribution. The majority of sources had a ^{12}CO 3–2 flux contribution under 20 per cent. However, in regions of molecular outflows, the ^{12}CO can dominate the source dust continuum (up to 79 per cent contamination) with ^{12}CO fluxes reaching ∼68 mJy beam^{-1}.

Key words: instrumentation: detectors – stars: formation – dust, extinction – ISM: jets and outflows – ISM: molecules – submillimetre: general.

1 INTRODUCTION

Dust continuum is a useful tracer of star formation. The submillimetre (roughly 300–1000 μm) detection of the dust emission identifies Class 0 and pre-stellar cores as well as discs, filamentary structure in molecular clouds, and the dust and gas masses of galaxies. In order to quantify the flux from dust in the submillimetre wavelengths, the heat generated by the radiation is measured by bolometers with the detected wavelength range defined by wide-band filters (Holland, Duncan & Griffin 2002). These observations of broad-band continuum emission from the dust can be contaminated by molecular line flux, particularly from ^{12}CO, which is the second most abundant molecule in the interstellar medium (after H_2) with strong emission lines in the submillimetre (Johnstone, Boonman & van Dishoeck 2003; Zhu, Seaquist & Kuno 2003; Seaquist et al. 2004; Hatchell & Dunham 2009). Since the molecular line contamination depends explicitly on the bandwidth and wavelength of the bolometer, it is important to quantify the potential contribution from molecular lines to make accurate flux measurements of the submillimetre dust emission used to calculate masses.

The CO line contribution can be quantified by comparing observations of the dust continuum emission and the CO line emission (Gordon 1995). Past research (Johnstone & Bally 1999; Davis et al. 2000; Papadopoulos & Allen 2000; Tothill et al. 2002) has studied the Submillimetre Common-User Bolometer Array (SCUBA) at the James Clerk Maxwell Telescope (JCMT), where line contribution from the ^{12}CO 3–2 line was found to range from little to tens of per cent in the 850-μm band. Other studies have examined contamination in various bolometer instruments, including the Max-Planck Millimeter Bolometer array (MAMBO-II), Bolocam and Submillimetre High-Angular Resolution Camera (SHARC-II). The SHARC-II operates at the same wavelength range as SCUBA (450 and 850 μm), but also includes a 350-μm filter (780–910 GHz). The

⋆E-mail: emily@astro.ex.ac.uk

350 μm SHARC-II continuum could be potentially contaminated by the ^{12}CO 7–6 line (806 GHz) up to ∼20 per cent, similar to the ^{12}CO 3–2 contamination to the SCUBA 850 μm continuum (Hatchell & Dunham 2009). While Bolocam (operated at Caltech at 1.1 mm with a 250–300 GHz filter) has been designed to exclude ^{12}CO line contamination, the MAMBO-II (operated by the Max Planck Institut für Radioastronomie at 1.2 mm with a ∼210–290 GHz filter) includes ^{12}CO 2–1 (230 GHz) molecular line emission which could potentially increase flux at most a few per cent (Aguirre et al. 2011). Other possible contamination for Bolocam and MAMBO-II could result from other known molecular lines in clouds, including SiO 6–5 (∼260 GHz) and HCN 3–2 (∼258 GHz).

The successor to SCUBA is SCUBA-2, a 10 000 pixel submillimetre camera on the JCMT with eight subarrays. SCUBA-2 operates at 450 and 850 μm, like SCUBA, and can be susceptible to significant molecular line contamination. In regards to ^{12}CO, both SCUBA-2 bandpass filters have a central transmission peak near a ^{12}CO line: the 850 μm bandpass filter centre is at 347 GHz near the ^{12}CO 3–2 line at 345.796 GHz and the 450 μm bandpass filter centre is 664 GHz near the ^{12}CO 6–5 line at 691.473 GHz. The proximity of the ^{12}CO line frequencies to the centres of the transmission peaks makes significant CO contamination in SCUBA-2 maps likely.

In this paper, we have calculated conversion factors used to convert maps of molecular line integrated intensity (K km s^{-1}) to maps of molecular line flux (mJy beam^{-1}) that contaminates the dust continuum emission. These conversion factors were calculated for ^{12}CO 3–2 contributions to the 850 μm SCUBA-2 dust continuum emission and for ^{12}CO 6–5 contributions to the 450 μm SCUBA-2 continuum. Conversion factors were applied to Heterodyne Array Receiver Programme (HARP) ^{12}CO maps of NGC 1333, a region in the Perseus molecular cloud complex, and NGC 2071 and NGC 2024, regions in the Orion B molecular cloud complex, to calculate the contamination directly by measuring fluxes and masses from a list of sources. Once the ^{12}CO contamination to the source fluxes was calculated, the sources with the highest contamination were analysed in more detail to determine the cause of the molecular flux contribution, e.g. molecular outflows or hot molecular gas from nearby stars.

This paper has six sections. In Section 2, we give details of the calculation of the conversion factors considering different weather grades (Section 2.1). Section 3 presents the resulting conversion factors calculated for ^{12}CO 3–2 (contributing to the 850 μm continuum band) and ^{12}CO 6–5 (contributing to the 450 μm continuum band). Section 4 explains how the conversion factors were applied to HARP ^{12}CO 3–2 maps to quantify the amount of contamination to the 850 μm SCUBA-2 dust continuum maps of three regions: NGC 1333, NGC 2071 and NGC 2024. Sections 4.1 and 4.2 introduce flux and mass calculations for a list of sources in the regions, and Section 4.3 presents further analysis of sources with high ^{12}CO contamination. Section 5 discusses the results, including the effects of environment and location (molecular outflows and hot ambient gas from nearby stars) on the ^{12}CO source contamination. This section also includes estimates of the ^{12}CO 6–5 line to the 450 μm SCUBA-2 dust emission. Finally, Section 6 summarizes the conclusions drawn from this work.

2 METHOD

Molecular line emission is typically measured as an intensity or surface brightness in terms of the Rayleigh–Jeans (R–J) brightness temperature (in kelvin), while the dust continuum fluxes are given in jansky measured over the telescope beam area (Jy beam^{-1}). In order to convert ^{12}CO line intensities to pseudo-continuum fluxes, the intensity of a molecular line must be converted into the flux of the line using the following relation:

$$F = \int I \, \mathrm{d}\Omega \approx I\Omega, \tag{1}$$

where I is the intensity and Ω is the telescope beam area. The intensity is measured as a main-beam brightness temperature $T_{\rm MB}$ in kelvin and converted to intensity using

$$I_\nu = \frac{2\nu^2}{c^2} k T_{\rm MB} = \frac{2k}{\lambda^2} T_{\rm MB}, \tag{2}$$

where ν is the frequency, λ is the wavelength and k is the Boltzmann constant.

A narrow molecular line within a filter contributes flux over a smaller frequency range ($\nu_{\rm line}$) than continuum emission across the filter. To obtain the flux from the molecular line, the average intensity $\langle I \rangle$ must be calculated over the full filter band, i.e.

$$\langle I \rangle = \frac{\int I_\nu(\mathrm{line})\, g_\nu(\mathrm{line})\, \mathrm{d}\nu}{\int g_\nu \, \mathrm{d}\nu}, \tag{3}$$

where I_ν(line) is the intensity of the molecular line, g_ν(line) is the filter passband (transmission) at the frequency of the molecular line and $\int g_\nu \, d\nu$ is the integrated filter passband (transmission) across the full range of filter frequencies. Using equation (2) and the Doppler shift, $\Delta\nu/\nu = \Delta v/c$, equation (3) can be converted to $T_{\rm MB}$:

$$\langle I \rangle = \frac{\frac{\nu}{c}\int I_\nu(v)\, g_\nu(v)\, \mathrm{d}v}{\int g_\nu \, \mathrm{d}\nu} = \frac{2k\nu^3}{c^3} \frac{g_\nu(\mathrm{line})}{\int g_\nu \, \mathrm{d}\nu} \int T_{\rm MB} \, \mathrm{d}v, \tag{4}$$

where $\int T_{\rm MB} \, \mathrm{d}v$ is the velocity integrated main-beam brightness temperature, or integrated intensity. Using these calculations of intensity, it follows from equation (1) that

$$\frac{F_\nu}{\mathrm{mJy\ beam^{-1}}} = \frac{2k\nu^3}{c^3} \frac{g_\nu(\mathrm{line})}{\int g_\nu \, \mathrm{d}\nu} \Omega_{\rm B} \int T_{\rm MB} \, \mathrm{d}v. \tag{5}$$

A similar calculation was used in Seaquist et al. (2004).

The main-beam brightness temperature $T_{\rm MB}$ is used rather than the antenna temperature $T_{\rm A}^*$ for analysing small-scale emission as long as the continuum calibration accounts for the same beam efficiencies as the molecular line emission. This is true for the SCUBA-2 and HARP pairing at the JCMT. The beam efficiencies are discussed further in Section 4. $T_{\rm A}^*$ is related to $T_{\rm MB}$ by the following:

$$T_{\rm A}^* = \eta_{\rm MB} T_{\rm MB}, \tag{6}$$

where $\eta_{\rm MB}$ is the main-beam efficiency factor. The efficiency factor that takes into account emission at larger scales is discussed in Section 2.2. At ∼345 GHz with HARP on JCMT, $\eta_{\rm MB}$ is 0.61 (Buckle et al. 2009). The telescope beam area, also discussed further in Section 2.2, is measured in steradians (sr) and obtained from the full width at half-maximum (FWHM) $\theta_{\rm B}$ of a Gaussian beam using $\Omega_{\rm B} = 2\pi\sigma^2$ where the FWHM $\theta_{\rm B} = 2\sqrt{2\ln 2}\sigma$:

$$\frac{\Omega_{\rm B}}{\mathrm{sr}} = \frac{\pi}{4\ln 2} \left(\frac{\theta_{\rm B}}{\mathrm{arcsec}}\right)^2 \left(\frac{\pi}{180 \times 3600}\right)^2. \tag{7}$$

Using equation (5), a molecular line conversion factor, C, can be calculated to convert molecular line maps, measured in the velocity

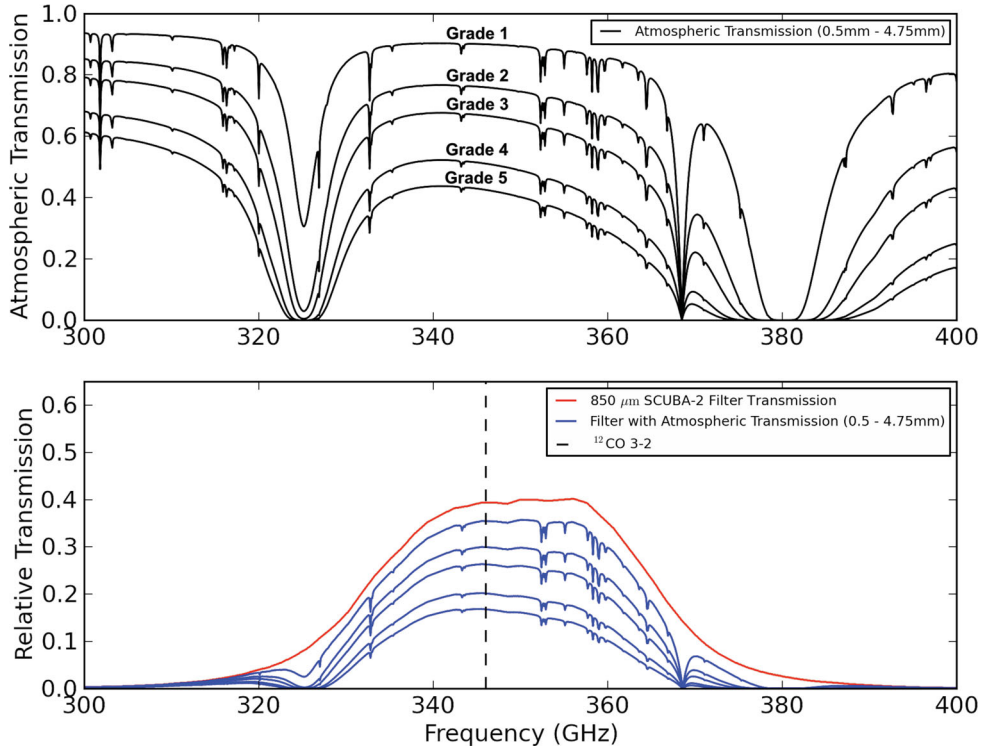

Figure 1. Top: plots of the atmospheric transmission at 300–400 GHz, given 0.5–4.75 mm of precipitable water vapour. Bottom: the upper line is the profile of the SCUBA-2 850 μm filter, and the lines beneath represent the SCUBA-2 filter with the addition of the atmospheric transmission at varying water vapour levels. The ^{12}CO 3–2 line is plotted at 345.7960 GHz. As shown in Table 1, the atmospheric transmission corresponds to different bands of weather used for observations.

integrated main-beam temperature $\int T_{\rm MB}\,{\rm d}v$ (K km s^{-1}), into maps of line flux (mJy beam^{-1}) that contributes to the observed continuum emission,

$$\frac{C}{\text{mJy beam}^{-1}\text{ per K km s}^{-1}} = \frac{F_\nu}{\int T_{\rm MB}\,{\rm d}v} = \frac{2k\nu^3}{c^3}\frac{g_\nu(\text{line})}{\int g_\nu\,{\rm d}\nu}\Omega_{\rm B}, \quad (8)$$

where frequencies are measured in GHz and 1 Jy = 10^{26} W m^2 Hz^{-1} = 10^{23} erg s^{-1} cm^{-2} Hz^{-1}. Note that the beam size is wavelength dependent, where $\Omega_{\rm B} \propto \lambda$. The difference in beam size between the ^{12}CO line and the SCUBA-2 filter is not taken into account.

2.1 Line conversion factors

To calculate the conversion factor C from equation (8), the SCUBA-2 filter profiles and the added atmospheric transmission were used to find $\int g_\nu\,{\rm d}\nu$ and g_ν(line). The SCUBA-2 850 and 450 μm filter profiles are shown in the bottom plot of Figs 1 and 2. The SCUBA-2 filter profiles are a result of stacking all of the filters (thermal and bandpass filters as well as the cryostat window and dichroic) that form the continuum bandpasses when combined with the atmosphere. The bandpasses are the main filters defining the transmission window, where passbands are the range of frequencies with a signal passing through the filter and stopbands define frequency ranges with a signal attenuated by the filter. The main infrared (IR; thermal) blocking filters are designed to block transmission at higher frequencies (IR and optical). For this study, a constant value for these filters has been assumed due to the high transmission in our frequency range. For further information, see the JCMT website regarding the cryostat window, filter and dichroic specification and measurements.[1]

The JCMT has a system that describes the atmospheric conditions ranging from weather grades 1 to 5. The atmospheric conditions are based on precipitable water vapour (PWV) levels (in mm) that correspond to different sky opacities at 225 GHz, or τ_{225}. The relation between PWV and τ_{225} is the following (JCMT overview website):[2]

$$\tau_{225} \approx 0.01 + (0.04 \times \text{PWV}). \quad (9)$$

The JCMT weather grades are defined as

(i) Grade 1: PWV: <1 mm, τ_{225}: <0.05;
(ii) Grade 2: PWV: 1 to 1.75 mm, τ_{225}: 0.05 to 0.08;
(iii) Grade 3: PWV: 1.75 to 2.75 mm, τ_{225}: 0.08 to 0.12;
(iv) Grade 4: PWV: 2.75 to 4.75 mm, τ_{225}: 0.12 to 0.20;
(v) Grade 5: PWV: >4.75 mm, τ_{225}: >0.20.

The continuum bandpass transmission of the filter profile and atmosphere combined varies depending on atmospheric conditions. Therefore, the CO contamination was calculated based on these five weather grades. Plots of atmospheric transmission corresponding to these conditions can be found in the top half of Figs 1 and 2 and are labelled according to the respective water vapour levels (for more detail, see the Caltech Submillimeter Observatory (CSO) Atmospheric Transmission Interactive Plotter website).[3] The SCUBA-2 850 and 450 μm filter profiles were multiplied by each individual atmospheric transmission profile to produce continuum bandpass

[1] http://www.jach.hawaii.edu/JCMT/continuum/scuba2/filter/
[2] www.jach.hawaii.edu/JCMT/overview/tel_overview
[3] http://www.submm.caltech.edu/cso/weather/atplot.shtml

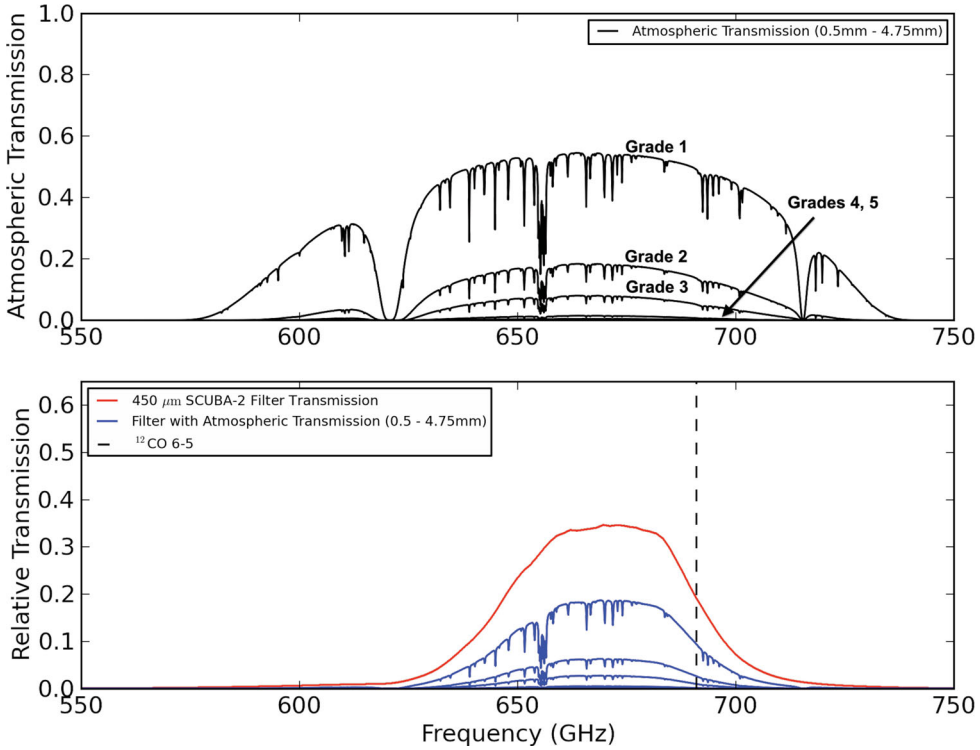

Figure 2. Top: plots of the atmospheric transmission at 550–750 GHz, given 0.5–4.75 mm of precipitable water vapour. Bottom: the upper line is the profile of the SCUBA-2 450 μm filter, and the lower lines represent the SCUBA-2 filter with the addition of the atmospheric transmission at varying water vapour levels. The ^{12}CO 6–5 line is plotted at 691.4731 GHz.

profiles at each weather grade, shown in the bottom plot of Figs 1 and 2.

In equation (5), $\int g_\nu \, \mathrm{d}\nu$ is the integrated SCUBA-2 continuum bandpass and is calculated as the sum of $g_\nu \times \delta\nu$ (where $\delta\nu$ is 0.01 GHz) at each corresponding frequency with units in GHz. The transmission of ^{12}CO, g_ν(line), is the transmission of the SCUBA-2 850 μm continuum bandpass at 345.7960 GHz (the rest frequency of the ^{12}CO 3–2 line) and the transmission of the SCUBA-2 450 μm continuum bandpass at 691.4731 GHz (the rest frequency of the ^{12}CO 6–5 line). To calculate conversion factors for redshifted lines, the frequency ν and transmission g_ν(line) (from Figs 1 and 2) in equation (8) must be changed appropriately. The SCUBA-2 beam size is calculated using equation (7) assuming that the main-beam FWHM θ_B is 13.8 arcsec at 850 μm and 8.3 arcsec at 450 μm. The possibility of an associated secondary beam is discussed in Section 2.2.

2.2 Telescope beam area

The beam profile of the original SCUBA instrument diverged from a single Gaussian and displayed a beam profile of two combined Gaussians: a primary beam roughly corresponding to the assumed FWHM and a secondary beam of 40 arcsec FWHM (Di Francesco et al. 2008). For the 450 μm maps, the primary beam had a 8.5 arcsec FWHM with a 0.90 relative amplitude and the secondary beam had a 0.10 relative amplitude. For the 850 μm maps, the primary beam had a 13.5 arcsec FWHM with a 0.96 relative amplitude and the secondary beam had a 0.04 relative amplitude.

It is possible that the total beam of SCUBA-2 also includes a broader secondary component. As explained in Section 2.1, the telescope beam areas for this study were calculated assuming FWHMs for the 450 μm (8.3 arcsec) and 850 μm (13.8 arcsec) SCUBA-2 beams. The primary beam is appropriate for studying the CO contamination in compact sources (small-scale emission), e.g. protostars and small outflows. However, if the CO emission is both bright and extended, then it may be necessary to include the secondary beam in the calculation. By fitting a two-component Gaussian to co-added SCUBA-2 maps of Uranus, the 450 μm primary FWHM is 8.7 arcsec (relative amplitude 0.83) and secondary FWHM is 20.4 arcsec (relative amplitude 0.17) and the 850 μm primary FWHM is 13.9 arcsec (relative amplitude 0.97) and secondary beam FWHM is 39.1 arcsec (relative amplitude 0.03).[4] The effective FWHM becomes 11.6 arcsec and 15.3 arcsec for 450 μm and 850 μm beams, respectively. This would cause the total beam area for 450 μm to be higher by a factor of 2.0 and the 850 μm total beam area to be higher by a factor of 1.2.

If it is necessary to incorporate the secondary beam into the beam area calculation, then a new conversion factor can be calculated using equation (8). The conversion factors are directly proportional to the telescope beam area. Assuming C' is the conversion factor with the inclusion of both a primary and secondary beam (Ω'_B) and C is the relation shown in equation (8), then it follows from equation (8):

$$C' = C\,\frac{\Omega'_\mathrm{B}}{\Omega_\mathrm{B}} = C\,\left(\frac{\mathrm{FWHM}'}{\mathrm{FWHM}}\right)^2, \qquad (10)$$

where FWHM′ is the effective FWHM. For large-scale and extended emission on scales significantly larger than the size of the telescope

[4] Measured primary beam sizes are slightly larger than the sizes quoted in Section 2.1. This is potentially due to small pointing shifts between co-added maps.

beam (greater than 13.8 arcsec, the 850 μm FWHM), it is also more appropriate to use $\eta_{\rm fss}$, the forward spillover and scattering efficiency, to calibrate the CO emission instead of the main-beam efficiency $\eta_{\rm MB}$. The forward spillover and scattering efficiency measure the amount of coupling to an extended source up to a 30 arcmin diameter (measured by observing the Moon). Equation (10) becomes

$$C' = C \left(\frac{\rm FWHM'}{\rm FWHM}\right)^2 \frac{\eta_{\rm MB}}{\eta_{\rm fss}}. \quad (11)$$

The increase of telescope beam area caused from the inclusion of the secondary beam is somewhat counterbalanced by the use of $T_{\rm R}^* = T_{\rm A}^*/\eta_{\rm fss}$ rather than $T_{\rm MB}$, accounting for the more efficient telescope coupling to large-scale emission ($\eta_{\rm fss} = 0.71$ compared to $\eta_{\rm MB} = 0.61$).

The secondary beam and potential changes in conversion factors for large-scale emission are further discussed in Section 5.

3 RESULTS

The ^{12}CO conversion factors, C, for SCUBA-2 are listed in Table 1. The ^{12}CO 3–2 conversion factors (in mJy beam^{-1} per K km s^{-1}) range from 0.63 (Grade 1) to 0.77 (Grade 5) with a mid-value of 0.70 (Grade 3). The conversion factors change depending on the atmospheric conditions that affect the continuum bandpass profile. Since each increase in τ_{225} causes the 850 μm continuum bandpass profile to become narrower with less overall transmission, $\int g_\nu {\rm d}\nu$ in equation (5) shrinks faster than the transmission of ^{12}CO, g_ν(line). Therefore, the ^{12}CO 3–2 line contribution to the flux is lowest in Grade 1 weather and steadily increases with each step to Grade 5 weather.

For the 450 μm continuum bandpass profile, the opposite trend is seen. The ^{12}CO line contribution to the 450 μm flux is highest in Grade 1 but steadily decreases with each step to Grade 5 weather. In most cases, observations using SCUBA-2 450 μm would only be taken in Grades 1 to 3 weather due to the decreased transmission in higher weather grades. The ^{12}CO 6–5 conversion factors range from 0.64 (Grade 1) to 0.35 (Grade 5) with a mid-value of 0.51 (Grade 3).

Note that the contamination is expected to have different behaviour between the 450 and 850 μm filters. The ^{12}CO 3–2 line is in the centre of the 850 μm filter with the bulk of the transmission, while the ^{12}CO 6–5 line is close to the edge of the 450 μm filter with lower transmission. The molecular line contribution to the 450 μm band decreases with weather grade because of the increasing attenuation of the ^{12}CO 6–5 line.

4 APPLICATIONS TO OBSERVATIONS

The conversion factors calculated in Section 3 were applied to HARP ^{12}CO 3–2 maps and compared to SCUBA-2 850 μm dust emission maps to measure the ^{12}CO contamination directly. Three different regions were used for this study: NGC 1333, NGC 2071 and NGC 2024. By quantifying the percentage of contamination to the dust continuum flux, we can determine regions more likely to be contaminated by CO (i.e. regions with molecular outflows or nearby stars).

4.1 Flux calculations

The continuum observations were taken with SCUBA-2 at 450 and 850 μm in each region in 2010 during the SCUBA-2 Shared Risk Observing (S2SRO) campaign when SCUBA-2 had two science grade arrays (one at 450 μm and one at 850 μm) installed. Observations were taken in Grade 2 weather conditions.

The HARP is a 16-pixel array receiver (16 receptors separated by 30 arcsec and a footprint of 2 arcmin). The ^{12}CO 3–2 data cube for NGC 1333 was observed in 2007 January using raster mapping techniques (for details see Curtis et al. 2010). The ^{12}CO 3–2 data cubes for NGC 2071 and NGC 2024 were observed in 2007 November using raster mapping techniques as well (see Buckle et al. 2010). Both data cubes were rebinned to 0.42 km s^{-1} velocity channels and converted to $T_{\rm MB}$ using a main-beam efficiency $\eta_{\rm MB}$ of 0.61.

Similar to other ground-based bolometer arrays, the limited, single-subarray version of SCUBA-2 available for S2SRO reproduced maps that are not sensitive to large-scale emission, in this case on scales larger than the single subarray field of view (∼4 arcmin). However, the HARP ^{12}CO maps still contain this large-scale flux. A simple application of the CO conversion factors from Table 1 to the HARP maps would retain the large-scale structure and overestimate the CO contamination. In order to account for the spatial filtering inherent in bolometer array reconstruction in a simple way and subtract the large-scale flux from the maps, a Gaussian smoothing mask (GSM) filter was applied to both the ^{12}CO HARP integrated intensity maps (in K km s^{-1}) and the 850 μm maps (mJy beam^{-1}) of the regions. The GSM filter was designed to minimize emission from structure on scales inaccessible to SCUBA-2 at this time. For the HARP maps, GSM filters were created by convolving a HARP ^{12}CO contamination map directly with a Gaussian a few arc minutes FWHM in size and subtracting the resulting smoothed map from the original map. For the SCUBA-2 maps, it was necessary to first create a thresholded map for masking bright protostars and

Table 1. Line contribution factors for ^{12}CO lines in the SCUBA-2 850 and 450 μm continuum bands.

Band	Filter with atmospheric trans. (PWV in mm)	$\int g_\nu {\rm d}\nu$ (GHz)	$\theta_{\rm B}$ (arcsec)	Line	ν (GHz)	g_ν(line)	τ_{225}	Weather grade	C (mJy beam^{-1} per K km s^{-1})
SCUBA-2 850 μm	0.5	19.79	13.8	^{12}CO 3–2	345.7960	0.58	0.03	1	0.63
	1.5	15.63	13.8	^{12}CO 3–2	345.7960	0.49	0.07	2	0.68
	2.25	13.24	13.8	^{12}CO 3–2	345.7960	0.43	0.10	3	0.70
	3.75	9.56	13.8	^{12}CO 3–2	345.7960	0.33	0.16	4	0.74
	4.75	7.71	13.8	^{12}CO 3–2	345.7960	0.28	0.20	5	0.77
SCUBA-2 450 μm	0.5	8.49	8.3	^{12}CO 6–5	691.4731	0.09	0.03	1	0.64
	1.5	2.64	8.3	^{12}CO 6–5	691.4731	0.02	0.07	2	0.57
	2.25	1.10	8.3	^{12}CO 6–5	691.4731	0.01	0.10	3	0.51
	3.75	0.19	8.3	^{12}CO 6–5	691.4731	<0.01	0.16	4	0.41
	4.75	0.06	8.3	^{12}CO 6–5	691.4731	<0.01	0.20	5	0.35

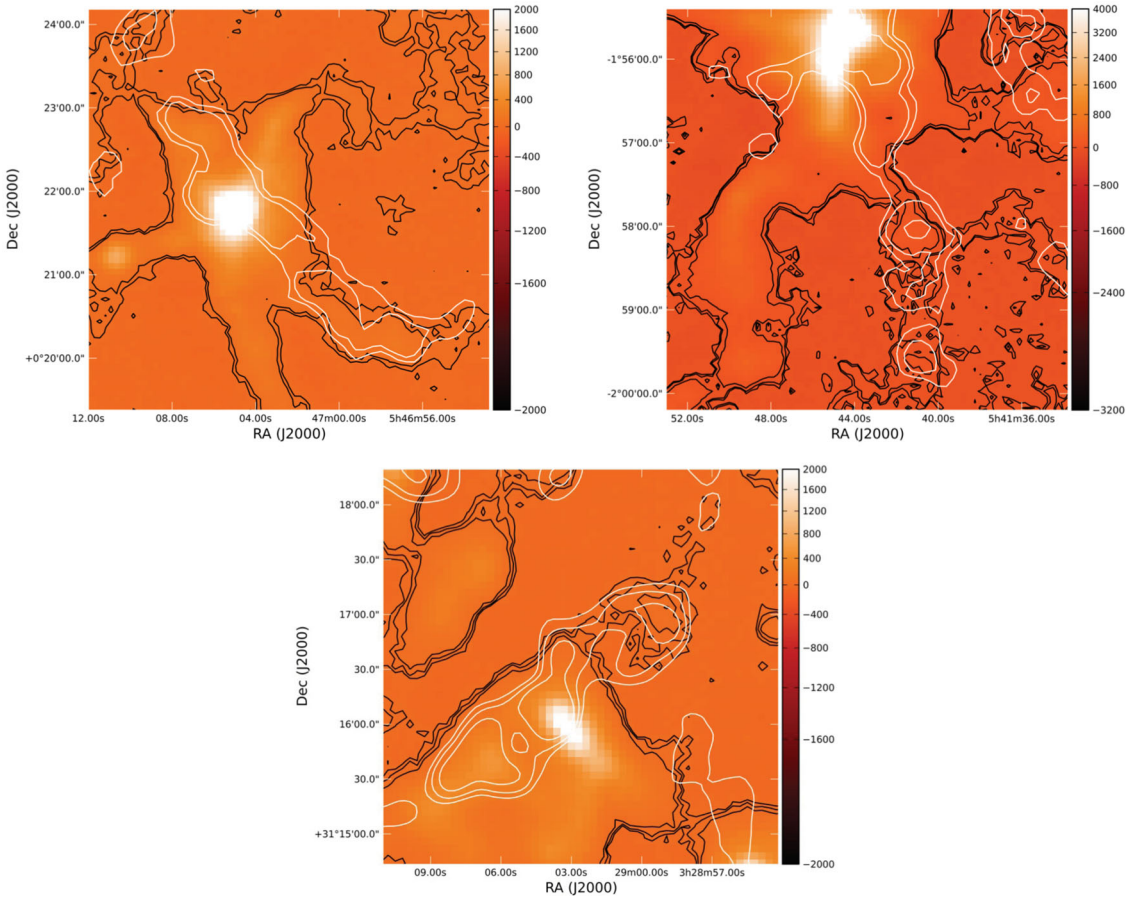

Figure 3. Regions in the SCUBA-2 850 μm GSM-filtered maps of NGC 2071, NGC 2024 and NGC 1333 where ^{12}CO emission contributes strongly to the 850 μm flux. Black contours correspond to the SCUBA-2 850 μm dust continuum maps and white contours correspond to HARP ^{12}CO 3–2 contamination maps. Top left: close-up of LBS-MM18 (NGC 2071-IRS) and corresponding outflow. Both sets of contours correspond to flux at 20 and 45 mJy beam^{-1}. Noticeable ^{12}CO flux contribution in the lower right lobe of the molecular outflow. Top right: close-up of FIR 1-7 and corresponding outflow. Both contours correspond to flux at 10, 20 and 45 mJy beam^{-1}. Noticeable ^{12}CO flux contribution in the lower lobe of the molecular outflow. Bottom: close-up of SVS13 and corresponding outflow. Both sets of contours correspond to flux at 10, 20 and 35 mJy beam^{-1}. Noticeable ^{12}CO flux contribution in the right lobe of the molecular outflow.

convolve the thresholded map with a Gaussian the same FWHM in size. The resulting smoothed map was then subtracted from the original map.

A 1 arcmin FWHM Gaussian was chosen for generating GSM maps after analysing 1–3 arcmin GSM filter sizes, further discussed in Section 4.1.4. Fig. 3 shows examples of the SCUBA-2 GSM processed maps for protostellar cores LBS-MM18 (NGC 2071-IRS) in NGC 2071 (see Motte et al. 2001), FIR 1-7 in NGC 2024 (see Richer et al. 1989; Buckle et al. 2010) and SVS13 in NGC 1333 (see Hatchell et al. 2007a). The brightest CO features in the maps are the result of molecular outflows driven by the dense cores in the regions. Dust emission contours in the outflows of these regions clearly follow the ^{12}CO 3–2 emission, indicating that the CO contamination is strong enough to be directly detected in the dust continuum.

To study the CO contamination quantitatively, aperture photometry with a 15 arcsec radius was applied to lists of known submillimetre sources, listed in Table 2 and further discussed in Sections 4.1.1–4.1.3. A 15 arcsec aperture radius was chosen based on source proximity and the possibility of the aperture diameter extending to a neighbouring source. Integrated flux densities are calculated by assuming a sky background of zero with flux uncertainties based on the sky rms and include a correction for the Gaussian beam (Enoch et al. 2006). Therefore, a point source has the same integrated flux density in any size aperture.

4.1.1 Application to NGC 1333

NGC 1333 is a reflection nebula in the Perseus molecular cloud and is characterized by early-stage star formation of age less than 1 Myr (Lada, Alves & Lada 1996; Wilking et al. 2004). The flux calibration for the S2SRO maps of this region was the CRL618 nebula and pointing checks were from the active galactic nucleus 3C84. A flux conversion factor (FCF) of 500 Jy beam^{-1} pW^{-1} was used for NGC 1333 to convert the maps into mJy beam^{-1}. Sources were chosen from a list of cores in NGC 1333 (Hatchell et al. 2007a) that had been previously identified in the submillimetre using SCUBA (Hatchell et al. 2005) and Bolocam (Enoch et al. 2006) with a total of 35 sources in the area covered by the SCUBA-2 map. These sources include a mixture of protostellar and starless cores. For further information regarding HARP observations, see Curtis et al. (2010).

Fig. 4 shows the source fluxes from the SCUBA-2 850 μm and ^{12}CO 3–2 Grade 2 contamination maps and the percentage contribution of ^{12}CO 3–2 flux to 850 μm SCUBA-2 flux. It should be noted that all of the sources have ^{12}CO contributions less than 20 per cent

Table 2. List of sources used for the study of ^{12}CO contamination to the SCUBA-2 850 μm dust continuum. Source numbers correspond to the arbitrary number assigned to sources for this study. Source numbers corresponding to original studies (NGC 1333 sources obtained from Hatchell et al. 2007a and NGC 2071 and NGC 2024 sources obtained from Nutter & Ward-Thompson 2007) are listed under 'Other Source ID'.

Region	Source	RA (J2000)	Dec. (J2000)	Other Source ID
NGC 1333	1	03:29:10.4	31:13:30	HRF41
	2	03:29:12.0	31:13:10	HRF42
	3	03:29:03.2	31:15:59	HRF43
	6	03:28:55.3	31:14:36	HRF44
	13	03:29:01.4	31:20:29	HRF45
	14	03:29:11.0	31:18:27	HRF46
	17	03:28:59.7	31:21:34	HRF47
	18	03:29:13.6	31:13:55	HRF48
	20	03:28:36.7	31:13:30	HRF49
	21	03:29:06.5	31:15:39	HRF50
	22	03:29:08.8	31:15:18	HRF51
	24	03:29:03.7	31:14:53	HRF52
	26	03:29:04.5	31:20:59	HRF53
	29	03:29:10.7	31:21:45	HRF54
	30	03:28:40.4	31:17:51	HRF55
	32	03:29:07.7	31:21:57	HRF56
	33	03:29:18.2	31:25:11	HRF57
	35	03:29:16.5	31:12:35	HRF59
	38	03:28:39.4	31:18:27	HRF60
	39	03:29:17.3	31:27:50	HRF61
	42	03:29:07.1	31:17:24	HRF62
	43	03:29:18.8	31:23:17	HRF63
	46	03:29:25.5	31:28:18	HRF64
	47	03:29:00.4	31:12:02	HRF65
	53	03:29:05.3	31:22:11	HRF66
	55	03:29:19.7	31:23:56	HRF67
	62	03:28:56.2	31:19:13	HRF68
	63	03:28:34.4	31:06:59	HRF69
	66	03:29:15.3	31:20:31	HRF70
	73	03:28:38.7	31:05:57	HRF71
	77	03:29:19.1	31:11:38	HRF72
	81	03:28:32.5	31:11:08	HRF74
	83	03:28:42.6	31:06:10	HRF75
	89	03:29:04.9	31:18:41	Bolo44
	94	03:28:32.7	31:04:56	Bolo26
NGC 2071	51	05:47:23.7	00:11:02	BN-547237+01102
	52	05:47:06.8	00:12:30	BN-547068+01230
	53	05:47:10.6	00:13:18	BN-547106+01318
	54	05:47:05.1	00:13:21	BN-547051+01321
	55	05:47:05.0	00:14:49	BN-547050+01449
	56	05:47:23.9	00:15:07	BN-547239+01507
	57	05:47:12.4	00:15:37	BN-547124+01537
	58	05:47:10.4	00:15:53	BN-547104+01553
	59	05:47:19.9	00:16:03	BN-547199+01603
	60	05:47:04.8	00:17:07	BN-547048+01707
	61	05:47:01.5	00:17:55	BN-547015+01755
	62	05:47:08.7	00:18:17	BN-547087+01817
	63	05:47:15.2	00:18:30	BN-547152+01830
	64	05:47:25.3	00:18:48	BN-547253+01848
	65	05:47:33.6	00:19:02	BN-547336+01902
	66	05:46:28.3	00:19:28	BN-546283+01928
	67	05:47:03.4	00:19:50	BN-547034+01950
	68	05:47:26.7	00:19:53	BN-547267+01953
	69	05:47:37.7	00:20:01	BN-547377+02001
	70	05:46:57.6	00:20:09	BN-546576+02009
	71	05:46:29.4	00:20:10	BN-546294+02010
	72	05:47:34.9	00:20:20	BN-547349+02020
	73	05:47:32.5	00:20:26	BN-547325+02026
	74	05:47:01.0	00:20:42	BN-547010+02042
	75	05:47:25.2	00:20:59	BN-547252+02059
	76	05:47:10.3	00:21:12	BN-547103+02112
	77	05:46:28.7	00:21:14	BN-546287+02114
	78	05:47:16.0	00:21:23	BN-547160+02123
	79	05:47:04.1	00:21:58	BN-547041+02158
	80	05:46:25.3	00:22:20	BN-546253+02220
	81	05:46:52.8	00:22:23	BN-546528+02223
	82	05:47:11.9	00:22:23	BN-547119+02223
	83	05:47:19.7	00:22:31	BN-547197+02231
	84	05:47:06.9	00:22:39	BN-547069+02239
	85	05:47:17.5	00:22:40	BN-547175+02240
	86	05:46:59.1	00:22:59	BN-546591+02259
	87	05:47:12.4	00:23:11	BN-547124+02311
	88	05:47:06.7	00:23:14	BN-547067+02314
	89	05:46:54.7	00:23:24	BN-546547+02324
	90	05:47:10.4	00:23:27	BN-547104+02327
	91	05:47:08.9	00:23:56	BN-547089+02356
	92	05:46:57.2	00:23:56	BN-546572+02356
	93	05:46:34.7	00:23:59	BN-546347+02359
	94	05:46:58.0	00:24:26	BN-546580+02426
	95	05:47:01.7	00:24:52	BN-547017+02452
	96	05:46:25.7	00:24:56	BN-546257+02456
	97	05:47:08.0	00:25:05	BN-547080+02505
	98	05:46:45.9	00:25:07	BN-546459+02507
	99	05:47:01.4	00:26:14	BN-547014+02614
	100	05:46:38.0	00:26:53	BN-546380+02653
NGC 2024	33	05 42 03.0	−02 04 23	BS-542030-20423
	34	05 42 10.3	−02 04 20	BS-542103-20420
	35	05 42 03.5	−02 02 24	BS-542035-20224
	36	05 41 57.1	−02 01 00	BS-541571-20100
	37	05 41 52.9	−02 00 21	BS-541529-20021
	38	05 41 49.3	−01 59 38	BS-541493-15938
	40	05 42 00.0	−01 58 01	BS-542000-15801
	41	05 41 49.1	−01 58 03	BS-541491-15803
	42	05 41 45.2	−01 56 31	BS-541452-15631
	43	05 41 35.4	−01 56 29	BS-541354-15629
	45	05 41 44.5	−01 55 39	BS-541445-15539
	46	05 41 44.2	−01 54 43	BS-541442-15443
	47	05 41 32.1	−01 54 26	BS-541321-15426
	48	05 41 19.9	−01 54 16	BS-541199-15416
	49	05 41 42.0	−01 53 59	BS-541420-15359
	51	05 41 44.2	−01 52 41	BS-541442-15241
	52	05 41 16.6	−01 51 19	BS-541166-15119
	53	05 41 36.7	−01 51 06	BS-541367-15106
	54	05 41 23.4	−01 50 27	BS-541234-15027
	55	05 41 32.9	−01 49 53	BS-541329-14953
	56	05 41 36.4	−01 49 24	BS-541364-14924
	57	05 41 27.6	−01 48 13	BS-541276-14813
	58	05 41 11.3	−01 48 12	BS-541113-14812
	59	05 41 13.3	−01 47 35	BS-541133-14735

and every source except one (source 21) has a contribution less than 10 per cent. Source 21 is further discussed in Section 4.3.

4.1.2 Application to NGC 2071

NGC 2071 is a region in the Orion B molecular cloud. Sources were chosen from a list of young stellar objects that had been previously

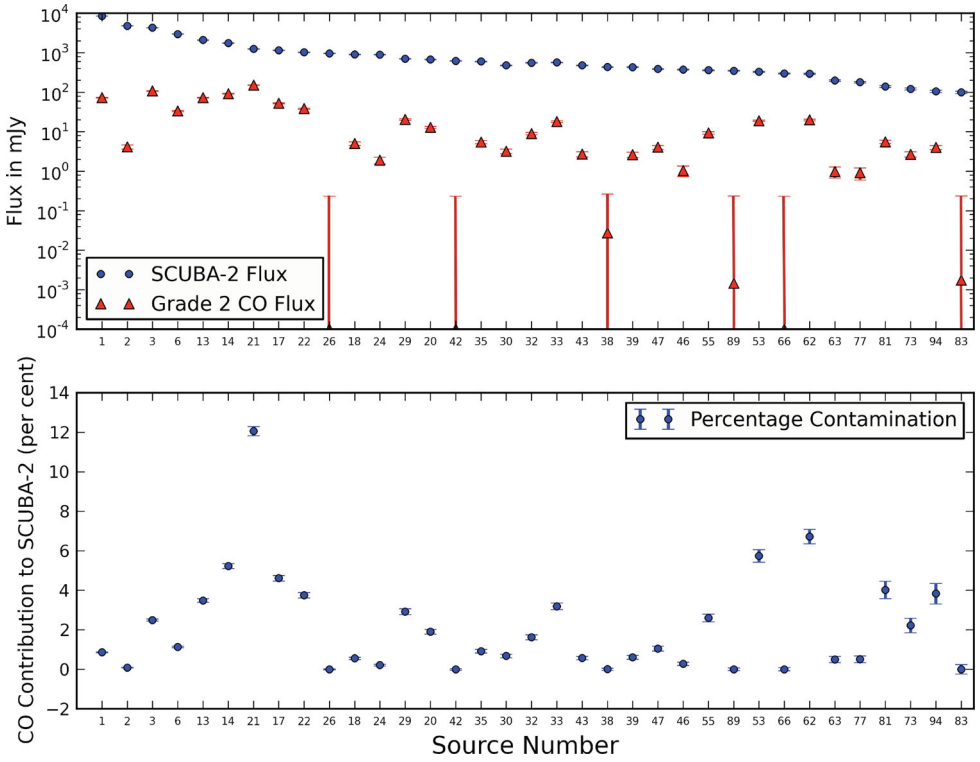

Figure 4. Top: the SCUBA-2 source fluxes calculated from the 850 μm continuum and ^{12}CO 3–2 contamination maps (Grade 2 weather) of NGC 1333. Note several sources (26, 42 and 66) have ^{12}CO flux contributions of 0 mJy beam^{-1}. Bottom: the percentage contribution to the SCUBA-2 fluxes from the ^{12}CO contamination maps. Numbers are given arbitrarily to the sources and were based on the original list of SCUBA and Bolocam cores (Hatchell et al. 2007a).

identified using SCUBA (Nutter & Ward-Thompson 2007) with a total of 50 sources in the area covered by the SCUBA-2 map. A FCF of 685 Jy beam^{-1} pW^{-1} was used for NGC 2071 as well as NGC 2024 (FCF value valid for 2010 October reduction, equivalent to Nutter et al., in preparation). For further information on HARP observations of NGC 2071, see Buckle et al. (2010).

Fig. 5 shows the source fluxes from the SCUBA-2 850 μm and ^{12}CO 3–2 Grade 2 contamination maps and the percentage contribution of ^{12}CO 3–2 flux to SCUBA-2 850 μm flux. Note that the majority of sources have ^{12}CO contributions of less than 20 per cent in Grade 2 weather. Four sources (sources 70, 74, 88 and 91) have ^{12}CO contributions greater than 20 per cent (ranging from 34 to 79 per cent). Sources with a higher ^{12}CO contamination are further discussed in Section 4.3.

4.1.3 Application to NGC 2024

NGC 2024 is another emission nebula in the Orion B molecular cloud. Sources were chosen from a list of young stellar objects in NGC 2024 that had been previously observed using SCUBA (Nutter & Ward-Thompson 2007) with a total of 24 sources in the area covered by the SCUBA-2 map. As stated in Section 4.1.2, a FCF of 685 Jy beam^{-1} pW^{-1} was used to correspond with current studies of Orion B (FCF value valid for 2010 October reduction, equivalent to Nutter et al., in preparation). For further information on HARP observations of NGC 2024, see Buckle et al. (2010).

Fig. 6 shows the source fluxes from the SCUBA-2 850 μm and ^{12}CO 3–2 Grade 2 contamination maps and the percentage contribution of ^{12}CO 3–2 flux to SCUBA-2 850 μm flux. Note that the majority of sources have ^{12}CO contributions of less than 20 per cent. One source (source 48) has a ^{12}CO contribution more than 20 per cent (34 per cent contamination), further discussed in Section 4.3.

4.1.4 GSM analysis

For SCUBA-2, GSM filters were created by applying upper thresholds to the original SCUBA-2 maps which acted as a mask for source emission and convolving the thresholded maps with a Gaussian a few arcminutes in FWHM size (similar to Reid & Wilson 2005; Kirk, Johnstone & Di Francesco 2006); this is a standard technique for the SCUBA-2 data. Negative regions of flux, known as negative 'bowls,' surround very strong sources in the SCUBA-2 maps and are produced in the map reconstruction process (see Johnstone et al. 2000). SCUBA-2 thresholding was necessary to prevent introducing new negative bowls in the image caused by smoothing and subtracting bright continuum sources. Without thresholding, artificial negative bowling would have been further added to the map, causing negative flux to lower source fluxes and increase the calculated ^{12}CO 3–2 contamination. To test the effects of changing the filter size, S2SRO maps were analysed with an upper threshold of 15 mJy beam^{-1} for NGC 1333 and 30 mJy beam^{-1} for NGC 2071 and NGC 2024 (used to mask out bright sources) and 1–3 arcmin FWHM Gaussian smoothing. Aperture fluxes from each of the GSM maps (1–3 arcmin) and the original, unsmoothed S2SRO maps were found to agree within uncertainties, indicating that the emission on scales which would have been affected by the GSM filter had been filtered out by the SCUBA-2 map reconstruction. The 1 and 2 arcmin GSM filters were further analysed with application to the HARP ^{12}CO maps based on the similarity between S2SRO and SCUBA maps, for which scales greater than 2 arcmin are known to be poorly reproduced (Hatchell et al. 2007a).

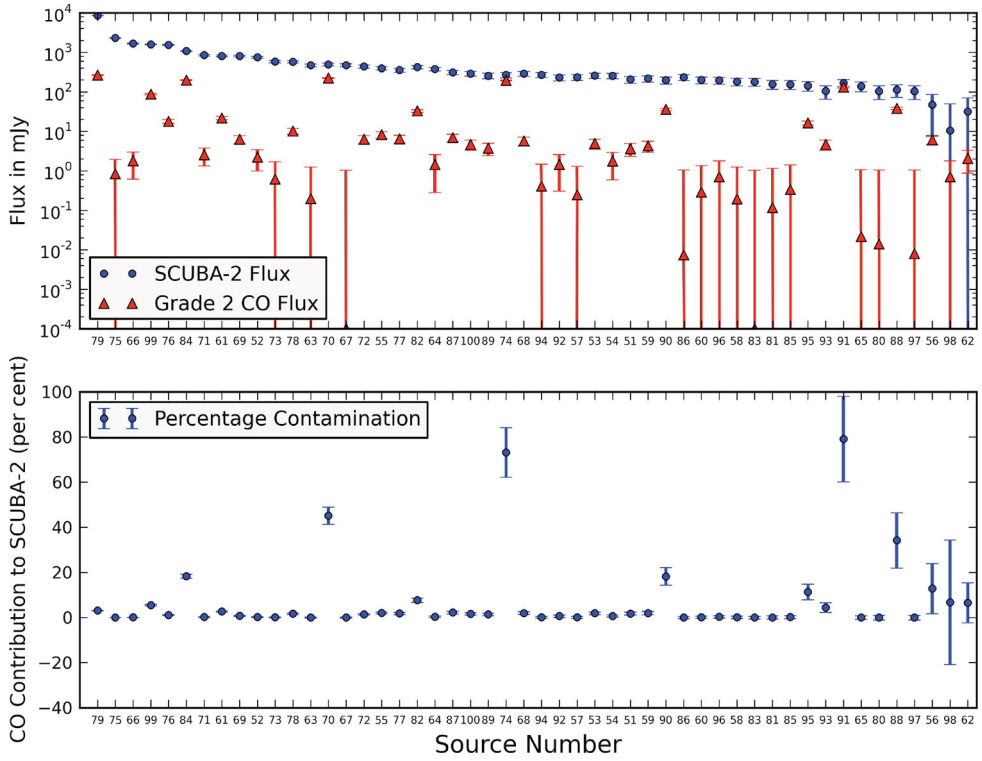

Figure 5. Top: the SCUBA-2 source fluxes calculated from the 850 μm continuum and ^{12}CO 3–2 contamination maps (Grade 2 weather) of NGC 2071. Note source 67 has a ^{12}CO flux contribution of 0 mJy beam^{-1}. Bottom: the percentage contribution to the SCUBA-2 fluxes from the ^{12}CO contamination maps. Numbers are given arbitrarily to the sources and were based on the original list of cores from Nutter & Ward-Thompson (2007).

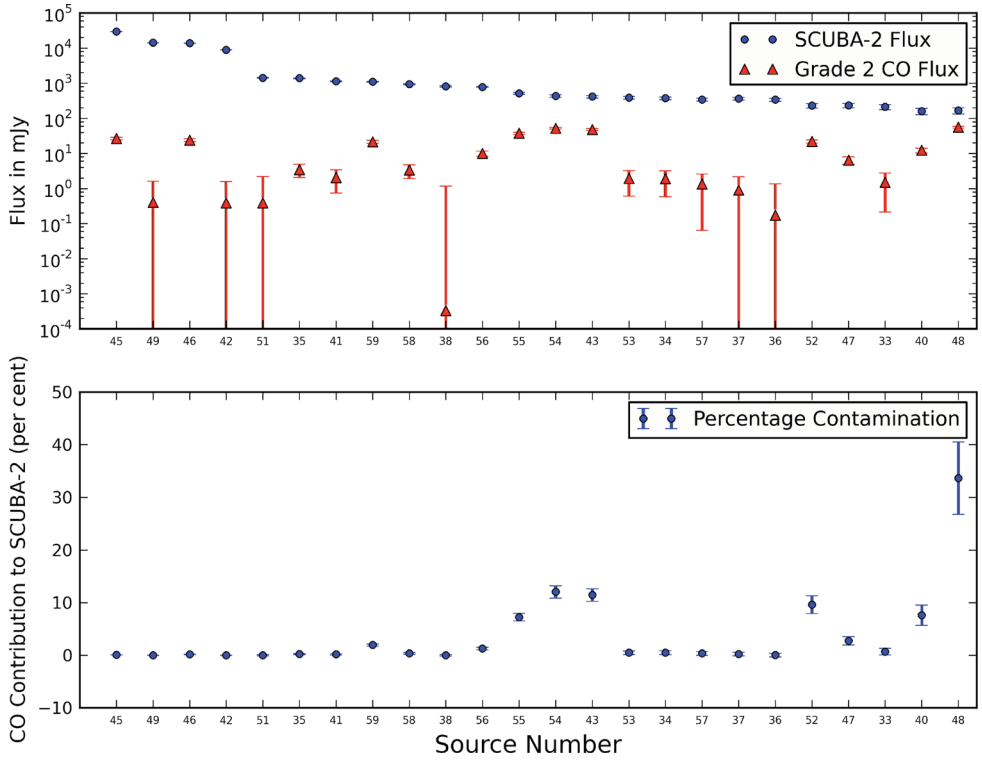

Figure 6. Top: the SCUBA-2 source fluxes calculated from the 850 μm continuum and ^{12}CO 3–2 contamination maps (Grade 2 weather) of NGC 2024. Bottom: the percentage contribution to the SCUBA-2 fluxes from the ^{12}CO contamination maps. Numbers are given arbitrarily to the sources and were based on the original list of cores from Nutter & Ward-Thompson (2007).

For the HARP ^{12}CO maps, thresholding was not required because ^{12}CO mainly traces molecular outflows which have bright, extended structures on scales not fully reproduced by SCUBA-2. To generate the ^{12}CO GSM maps, GSM filters with 1 and 2 arcmin FWHM Gaussians were directly applied and subtracted from the original maps. Negative flux regions in the final HARP maps resulting from the oversubtraction of background flux estimated by the GSM filter was set to 0 mJy beam^{-1} to prevent biasing the source fluxes in the aperture photometry process. The S2SRO 1 and 2 arcmin GSM maps were subtracted from the corresponding ^{12}CO GSM maps (Grade 2 contamination) to analyse the GSM filter effectiveness in matching the spatial filtering of the SCUBA-2 maps. Positive flux in the residuals indicates higher ^{12}CO flux than 850 μm dust continuum flux, suggesting that the GSM filter size should be scaled down to subtract smaller scale emission. In each of the regions, the 2 arcmin GSM residuals were found to overestimate the ^{12}CO flux contribution to the dust continuum. On average, the 2 arcmin GSM map residuals were 1.4 to 1.5 times greater than the 1 arcmin GSM. The 1 arcmin GSM filters were applied to both the S2SRO and HARP maps for consistency in eliminating flux on scales of 1 arcmin and above.

With the full complement of subarrays, SCUBA-2 is likely to recover more large-scale structure and continuum fluxes may increase further. A comparison of ^{12}CO contamination on scales of 1 arcmin or greater will have to wait for full SCUBA-2 operations.

4.2 Mass calculations

The calculation of the dust continuum flux from pre- and protostellar sources in a molecular cloud can be used to obtain source masses (Hildebrand 1983). Depending on the molecular cloud environment surrounding the sources, contamination from the ^{12}CO line emission may affect low- and high-mass sources, leading to a varying level of source contamination. Therefore, the masses of sources were calculated using the relation between the dust and gas mass and the total source dust continuum flux (e.g. Seaquist et al. 2004; Enoch et al. 2006),

$$M = \frac{S_{850} D^2}{\kappa_{850} B_{850}(T_{\rm d})}, \tag{12}$$

where S_{850} is the flux from 15 arcsec radius aperture photometry at 850 μm, D is the distance to the source, κ_{850} is the dust opacity at 850 μm and $B_{850}(T_{\rm d})$ is the Planck function at 850 μm for the dust temperature $T_{\rm d}$.

4.2.1 Mass calculations for NGC 1333

For NGC1333, a distance of 250 pc was assumed for the mass calculations. Hatchell et al. (2007a) used a distance of 320 pc, which would increase masses by a factor of 1.6. A temperature of 10 K was used as an estimate of the dust temperature, where dense regions that do not have internal heating are colder on the inside and warmer on the outside (Evans et al. 2001). Cores with internal heating are warmer in the inner regions. For example, Class 0 and Class I protostars are found from models to have $\sim T_{\rm d} = 15$ K (Shirley, Evans & Rawlings 2002; Young et al. 2003), but most of the dust mass is found in areas of lower temperatures. To cover pre- and protostellar sources, $T_{\rm d} = 10$ K is a commonly used average. It should be noted that this value can overestimate the masses of protostellar sources by a factor of 2–3 if the temperature is warmer (Enoch et al. 2006).

The dust opacity κ_{850} is also uncertain for individual regions. Hatchell et al. (2007a) assumed a dust opacity of 0.012 cm^2 g^{-1} for the 850 μm SCUBA dust emission maps of NGC 1333 based on a gas/dust ratio of 161 (see Ossenkopf & Henning 1994). This dust opacity is at the low end of the assumed values and a dust opacity of 0.02 cm^2 g^{-1} at 850 μm could have been used (Kirk et al. 2006). Here, we choose a dust opacity of 0.012 cm^2 g^{-1}. If 0.02 cm^2 g^{-1} were used, then our masses would decrease by a factor of 1.7.

Masses were calculated from source fluxes obtained from continuum emission with and without ^{12}CO contamination taken into account. The bottom portion of Fig. 7 shows the ratio between these masses. Due to the CO flux contamination, the calculated source masses are being overestimated by up to a factor of 1.2.

4.2.2 Mass calculations for NGC 2071 and NGC 2024

For NGC 2071 and NGC 2024, parameters from past mass estimates (Nutter & Ward-Thompson 2007) were used to calculate source masses. A distance of 400 pc was assumed for both regions (Brown, de Geus & de Zeeuw 1994) and a temperature of 20 K was assumed as an estimate of the dust temperature (Launhardt et al. 1996; Mitchell et al. 2001; Johnstone & Bally 2006). An 850 μm dust opacity of 0.01 cm^2 g^{-1} was used (Andre, Ward-Thompson & Motte 1996; Ward-Thompson, Motte & Andre 1999; André et al. 2003), similar to the dust opacity used for NGC 1333. As in NGC 1333, the assumption of a single temperature for each source does introduce a potential bias in the masses. If 10 K was assumed, as for NGC 1333, then masses for NGC 2071 and NGC 2024 sources would be larger by a factor of 2.

Masses were calculated from the source fluxes of the 850 μm continuum emission (see Section 4) with and without ^{12}CO 3–2 contribution taken into account. The bottom portion of Figs 8 and 9 show the ratio between these masses for NGC 2071 and NGC 2024, respectively. Due to the CO flux contamination, the calculated source masses are being overestimated by a factor up to 4.8 for NGC 2071 and 1.5 for NGC 2024.

4.3 Molecular outflow analysis

The location of protostellar sources can help identify the potential causes of ^{12}CO contamination. The presence of protostellar molecular outflows and hot ambient gas from nearby stars results in bright ^{12}CO emission, making regions with these characteristics rife with CO contamination.

Sources with high ^{12}CO contamination were examined in further detail using the HARP data cubes. In each of the three regions, sources with greater than 20 per cent contamination were defined as 'sources with high contamination'. For NGC 1333, there were no sources with greater than 20 per cent contamination, excluding it from this portion of the high contamination study. In NGC 2071, four sources fulfilled the high contamination criterion and one source in NGC 2024 fulfilled the criterion. In order to identify the cause of high contamination, the ^{12}CO spectra were extracted and analysed for molecular outflows.

For NGC 2071 and NGC 2024, the line wing criterion used to identify a molecular outflow candidate was a line wing above 1.5 K ($T_{\rm A}^*$) at ±4 km s^{-1} from the core velocity, $v_{\rm LSR}$. This line wing criterion method follows the method in Hatchell, Fuller & Richer (2007b). A core velocity of 10 km s^{-1} was used for all of the sources in NGC 2024 and NGC 2071 based on C^{18}O 3–2 data (Buckle et al. 2010). Line wing criteria were based on $T_{\rm A}^*$ rms values for the regions (5σ).

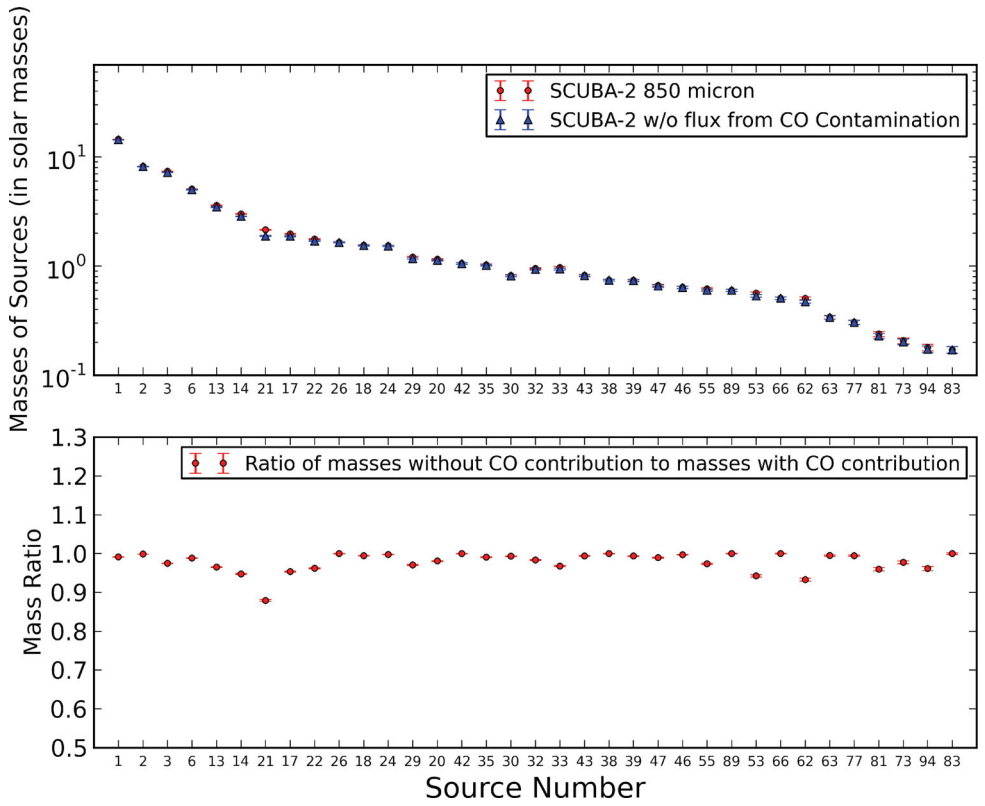

Figure 7. Top: mass calculations (in solar masses) of the different sources in NGC 1333. The masses were calculated using the SCUBA-2 850 μm map and then recalculated excluding the flux contribution from ^{12}CO in different atmospheric conditions. Bottom: ratio of the masses calculated from the flux without to with the ^{12}CO contribution. In both plots, uncertainties are calculated only from the source fluxes and do not include absolute calibration uncertainties.

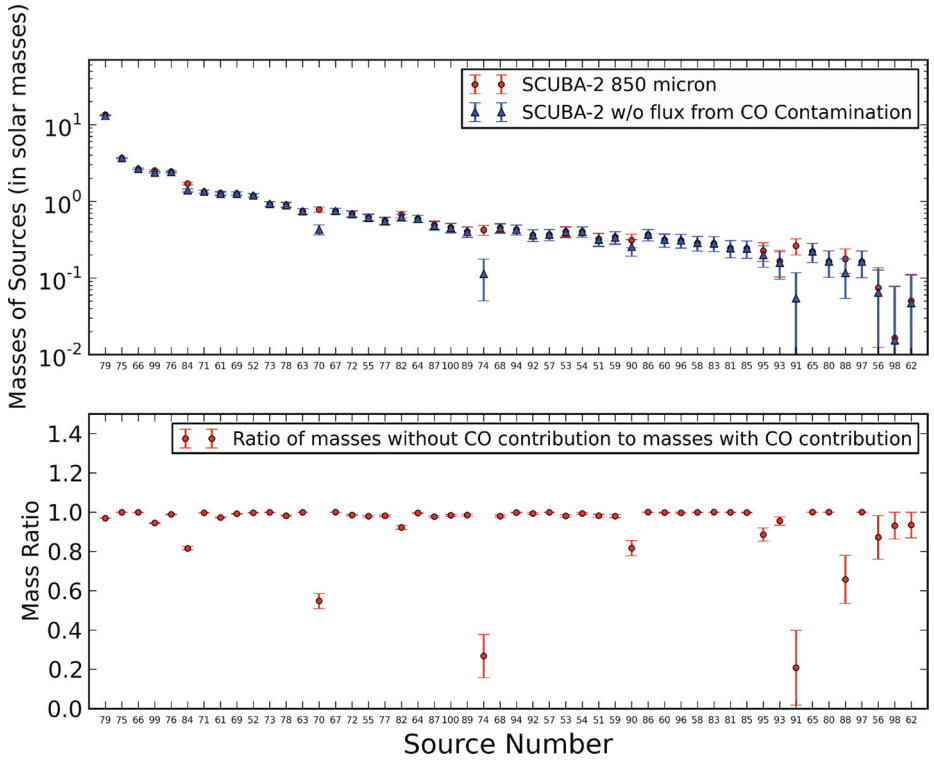

Figure 8. Top: mass calculations (in solar masses) of the different sources in NGC 2071. The masses were calculated using the SCUBA-2 850 μm map and then recalculated excluding the flux contribution from ^{12}CO in different atmospheric conditions. Bottom: ratio of the masses calculated from the flux without to with the ^{12}CO contribution. In both plots, uncertainties are calculated only from the source fluxes and do not include absolute calibration uncertainties.

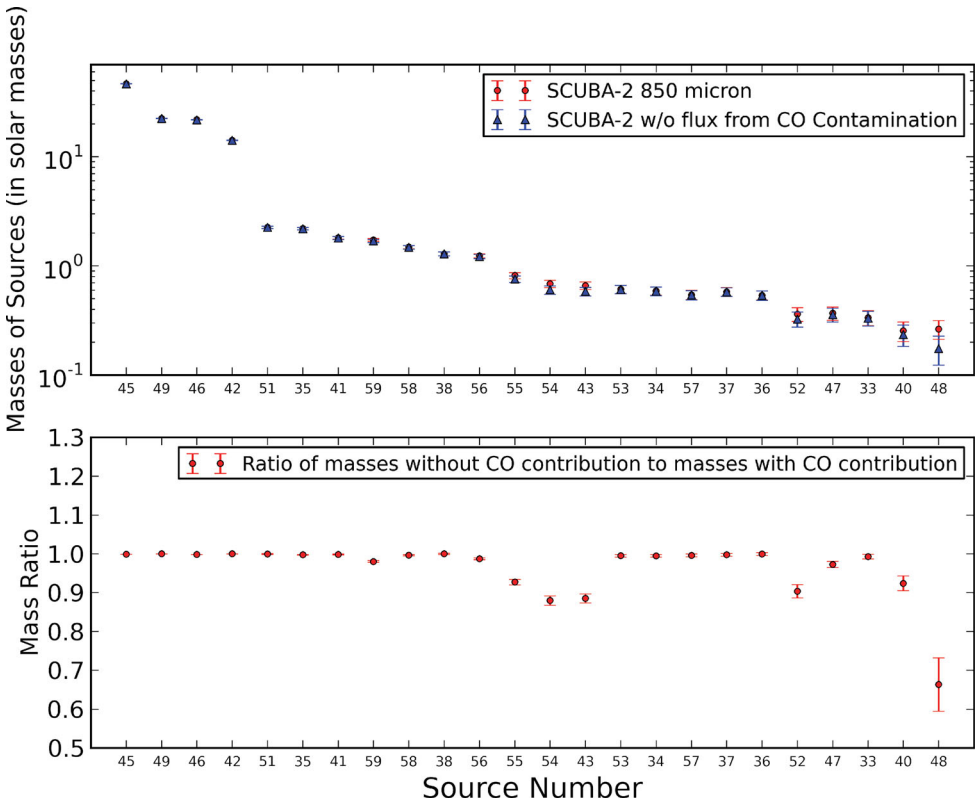

Figure 9. Top: mass calculations (in solar masses) of the different sources in NGC 2024. The masses were calculated using the SCUBA-2 850 μm map and then recalculated excluding the flux contribution from ^{12}CO in different atmospheric conditions. Bottom: ratio of the masses calculated from the flux without to with the ^{12}CO contribution. In both plots, uncertainties are calculated only from the source fluxes and do not include absolute calibration uncertainties.

The line wing criterion identifies not only protostars driving molecular outflows, but also sources which are contaminated by outflows along the line of sight. Outflow candidates were identified using the above criteria and examined further to determine if the source or another protostar was the outflow driving source. Sources with high contamination that were not outflow candidates were further analysed to determine if there were other causes behind the ^{12}CO contamination, such as a nearby star heating the gas.

Highly contaminated sources are listed in Table 3. Table 3 includes the region, source number, RA and Dec., flux calculated from aperture photometry in mJy, ^{12}CO flux contamination in Grade 2 weather in mJy, percentage contamination from ^{12}CO, core velocity $v_{\rm LSR}$ in km s^{-1} and the final molecular outflow candidate result. The outflow naming convention follows Hatchell & Dunham (2009), where a 'y' is given when an outflow is present. Sources are marked '?' when there is confusion as to the source of the outflow. In this case, the potential source causing the outflow detection is listed in a footnote.

4.3.1 *Sources in NGC 1333*

Fig. 10 shows the 850 μm SCUBA-2 map with blue contours tracing the blueshifted ^{12}CO HARP intensity $\int T_{\rm A}^{*}\,{\rm d}v$ (integrated from −2.5 to 4.5 km s^{-1}) and red contours tracing the redshifted ^{12}CO intensity (integrated from 10.5 to 16.5 km s^{-1}). Sources in NGC 1333 are denoted by the percentage contamination, where '×' denotes sources with 0–10 per cent contamination and '+' denotes sources with 10–20 per cent contamination. Source 21 had the highest

Table 3. List of sources categorized with high ^{12}CO contamination to the 850 μm dust continuum.

Region	Source	RA (J2000)	Dec. (J2000)	Flux[a] (mJy)	^{12}CO (Grade 2) (mJy)	Percentage cont. (Grade 2)	$v_{\rm LSR}$ (km s^{-1})	Outflow?
NGC 2071	70	05:46:57.6	00:20:09	495 ± 40	224 ± 6	46 ± 5	10.0	y
	74	05:47:01.0	00:20:42	268 ± 40	196 ± 6	73 ± 13	10.0	y
	88	05:47:06.7	00:23:14	112 ± 39	38 ± 3	34 ± 14	10.0	y?[b]
	91	05:47:08.9	00:23:56	166 ± 40	132 ± 5	79 ± 22	10.0	y?[b]
NGC 2024	48	05:41:19.9	−01:54:16	168 ± 33	56 ± 3	34 ± 9	10.0	y

[a]SCUBA-2 fluxes appear to be lower than seen by SCUBA due to the subtraction of large-scale flux by SCUBA-2.
[b]Could be due to a large, central blue outflow from source at (J2000) 05:47:06.9, 00:22:39 (source 84; LBS-MM19) or a source at (J2000) 05:47:04.1, 00:21:58 (LBS-MM18; NGC 2071-IRS), where LBS-MM18 was found to be responsible for driving the outflow in Motte et al. (2001) and both sources are confirmed Class 1 protostars detected using IRAC (Nutter & Ward-Thompson 2007).

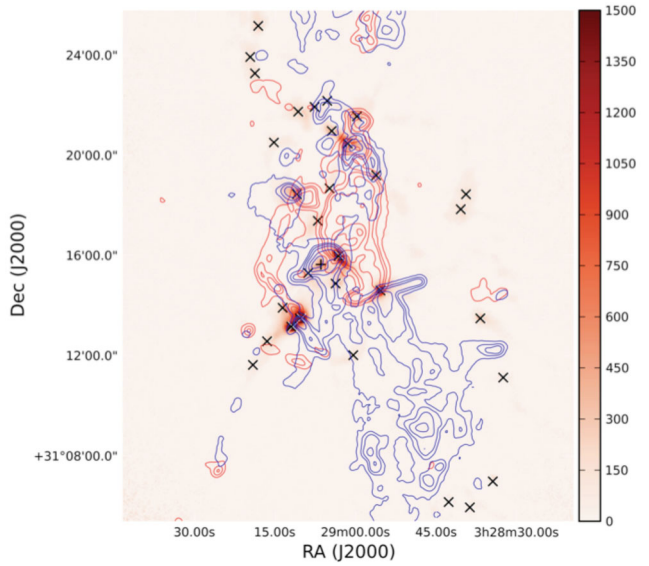

Figure 10. SCUBA-2 850 μm map of NGC 1333. The colour bar represents flux in mJy beam^{-1}. Blue contours correspond to blueshifted ^{12}CO 3–2 HARP intensity $\int T_{\rm A}^{*}\,{\rm d}v$ (integrated from −2.5 to 4.5 km s^{-1}). Red contours correspond to redshifted intensity (integrated from 10.5 to 16.5 km s^{-1}). Contour levels are 5, 10, 15, 25, 45, 65 and 85 K km s^{-1}. Sources in NGC 1333 are denoted by percentage contamination, where '×' denotes sources with 0–10 per cent contamination and '+' denotes sources with 10–20 per cent contamination.

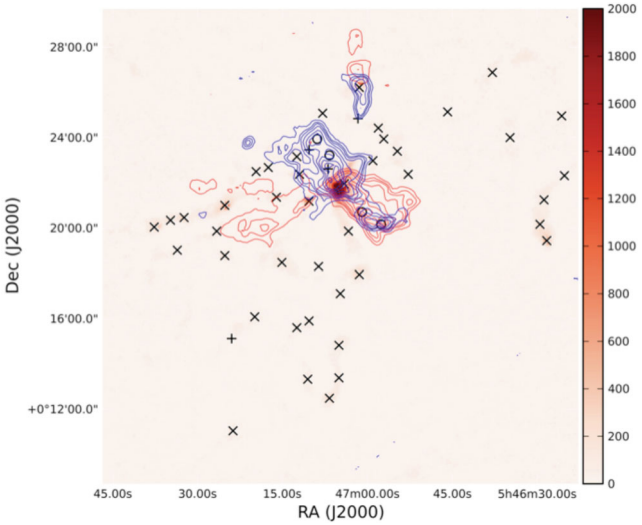

Figure 11. SCUBA-2 850 μm map of NGC 2071. The colour bar represents flux in mJy beam^{-1}. Blue contours correspond to blueshifted ^{12}CO 3–2 HARP intensity $\int T_{\rm A}^{*}\,{\rm d}v$ (integrated from −2.0 to 6.0 km s^{-1}). Red contours correspond to redshifted intensity (integrated from 14.0 to 22.0 km s^{-1}). Contour levels are 5, 10, 15, 25, 45, 65, 85, 105, 125 and 145 K km s^{-1}. Sources in NGC 2071 are denoted by percentage contamination, where '×' denotes sources with 0–10 per cent contamination, '+' denotes sources with 10–20 per cent contamination, and 'O' denotes sources with greater than 20 per cent contamination.

percentage contamination at 12 per cent. According to the line wing criteria used to identify a molecular outflow candidate (line wing above 1.5 K for $T_{\rm A}^{*}$ at ±3 km s^{-1} from the core velocity 7.9 km s^{-1}, following the criterion for NGC 1333 used in Hatchell et al. 2007b), source 21 is a molecular outflow candidate that could potentially be the result of a source at (J2000) 03:29:03.2, 31:15:59.0 (SVS13) or source at (J2000) 03:29:08.8, 31:15:18.1 (SK-16) (Hatchell & Dunham 2009). A ^{12}CO spectrum for this source is included in Fig. A1.

4.3.2 Sources in NGC 2071

Fig. 11 shows 850 μm SCUBA-2 map with blue contours tracing the blueshifted ^{12}CO HARP intensity $\int T_{\rm A}^{*}\,{\rm d}v$ (integrated from −2.0 to 6.0 km s^{-1}) and red contours tracing the redshifted ^{12}CO intensity (integrated from 14.0 to 22.0 km s^{-1}). Sources in NGC 2071 are denoted by the percentage contamination, where '×' denotes sources with 0–10 per cent contamination, '+' denotes sources with 10–20 per cent contamination and 'O' denotes sources with greater than 20 per cent contamination. According to the line wing criteria used, all four sources with high contamination are molecular outflow candidates. Even though sources 70 and 74 have clear blue- and redshifted spectral line wings, all four sources appear to trace a large central outflow that could be driven by a source at (J2000) 05:47:06.9, 00:22:39 (source 84; LBS-MM19) or a source at (J2000) 05:47:04.1, 00:21:58 (source 79; LBS-MM18; NGC 2071-IRS), where LBS-MM18 was found to be responsible for driving the outflow in Motte et al. (2001) and both sources are confirmed Class 1 protostars detected using Infrared Array Camera (IRAC; Nutter & Ward-Thompson 2007). Note that sources 84 (LBS-MM19) and 90, both with 18 per cent contamination, also correlate with the central outflow. The ^{12}CO spectra for these sources are displayed in Fig. A1.

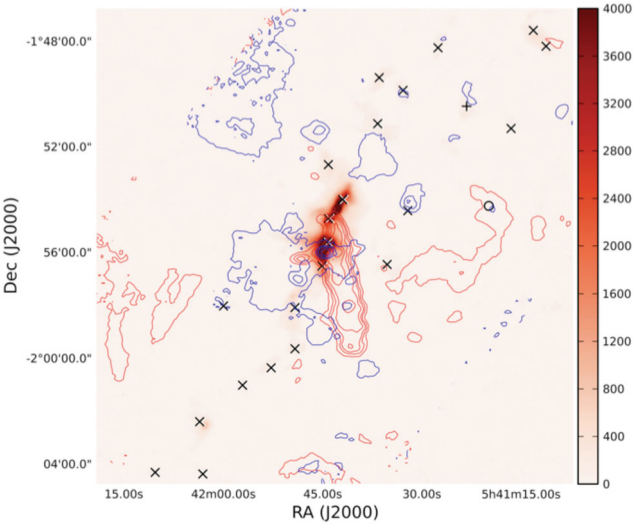

Figure 12. SCUBA-2 850 μm map of NGC 2024. The colour bar represents flux in mJy beam^{-1}. Blue contours correspond to blueshifted ^{12}CO 3–2 HARP intensity $\int T_{\rm A}^{*}\,{\rm d}v$ (integrated from −2.0 to 6.0 km s^{-1}). Red contours correspond to redshifted intensity (integrated from 14.0 to 22.0 km s^{-1}). Contour levels are 5, 10, 15, 25, 45, 65, 85, 105, 125 and 145 K km s^{-1}. Sources in NGC 2024 are denoted by percentage contamination, where '×' denotes sources with 0–10 per cent contamination, '+' denotes sources with 10–20 per cent contamination and 'O' denotes sources with greater than 20 per cent contamination.

4.3.3 Sources in NGC 2024

Fig. 12 shows 850 μm SCUBA-2 map with blue contours tracing the blueshifted ^{12}CO HARP intensity $\int T_{\rm A}^{*}\,{\rm d}v$ (integrated from −2.0 to 6.0 km s^{-1}) and red contours tracing the redshifted ^{12}CO intensity (integrated from 14.0 to 22.0 km s^{-1}). Sources in NGC 2024 are

denoted by the percentage contamination, where '×' denotes sources with 0–10 per cent contamination, '+' denotes sources with 10–20 per cent contamination and 'O' denotes sources with greater than 20 per cent contamination. According to the line wing criteria used, the single source with a high contamination is a molecular outflow candidate. The ^{12}CO spectrum for this source is listed in Fig. A1.

5 DISCUSSION

Typical ^{12}CO contamination levels in the observed SCUBA-2 850 μm emission from NGC 1333, NGC 2071 and NGC 2024 are under 20 per cent (this includes 95 per cent of sources, and 88 per cent of all sources have under 10 per cent contamination). Similar results were found for SCUBA, where Johnstone et al. (2003) suggested that ^{12}CO line contamination is typically under 10 per cent for submillimetre sources in Orion and Davis et al. (2000) suggested that contamination was ∼10 per cent near the source V380 Orion NE.

In locations where molecular outflows are present, ^{12}CO contamination can rise above 20 per cent and dominate the dust continuum (up to 79 per cent contamination), corresponding to a CO contribution ranging from 16 to 68 mJy beam^{-1} for the sources analysed in this study. Peak ^{12}CO fluxes found in the molecular outflows of NGC 1333, NGC 2071 and NGC 2024 maps reach even higher fluxes of 84, 154 and 94 mJy beam^{-1}, respectively. Our study suggests that molecular outflows can influence line contamination in sources with both high and low continuum fluxes (∼100–500 mJy). This result agrees with that of Johnstone et al. (2003), where they concluded that the areas with warmer molecular gas temperatures and higher velocities (i.e. shocks and molecular outflows) were the only locations where ^{12}CO emission dominated the dust continuum flux due to the higher molecular line integrated intensities associated with such regions. In addition, Gueth, Bachiller & Tafalla (2003) found a 20 per cent contamination for the well-known outflow source L1157. Hatchell & Dunham (2009) similarly found a 20–30 per cent ^{12}CO contamination level in the IRAS 03282+3035 outflow in Perseus.

The ^{12}CO contamination combined with contamination from other molecular lines allows outflows to potentially be seen in continuum maps with a similar appearance as protostellar cores or filamentary structure, which may be the case for SVS13 in NGC 1333 and the large, central outflows in NGC 2071 and NGC 2024 that have strong evidence of molecular outflow lobes detected in the dust continuum emission maps (see Fig. 3). Other studies have suggested that regions involving molecular outflows can reach 50 per cent ^{12}CO contamination, e.g. in the extended outflow lobes of V380 Orion NE (Davis et al. 2000), and even up to 100 per cent contamination, e.g. the central blue outflow region in NGC 2071 driven by source LBS-MM18 (NGC 2071-IRS; Motte et al. 2001).

The FCF uncertainty from calibrator observations for the 850 μm S2SRO maps is 18 per cent (SMURF SCUBA-2 Data Reduction Cookbook).[5] The calibration uncertainty of HARP observations at JCMT is estimated to be 20 per cent by Buckle et al. (2009). With contamination levels to SCUBA-2 850 μm less than or equal to 20 per cent for the majority of the sources, the typical contamination is less than or equivalent to the calibration uncertainty. Problems arise when the contamination is greater than calibration uncertainties, contributing a significant portion of flux and potentially dominating the dust continuum. For bright sources, it should be possible to use the subtracted ^{12}CO background to estimate the column density and hence the potential CO contamination to the 850 μm SCUBA-2 dust emission, as suggested by Tothill et al. (2002).

For faint sources, the insensitivity of SCUBA-2 to the large-scale dust emission introduces additional uncertainties. The spatially filtered maps created here do not appear to entirely subtract the total large-scale flux detected by HARP. Excess ^{12}CO flux seen as positive flux in residuals (Section 4.1.4) points to the need for a more detailed model of SCUBA-2 structure response. The large-scale reconstruction issues limit analysing contamination where the SCUBA-2 flux is faint. This analysis is something we will consider for the full SCUBA-2 array, but not for the limited S2SRO data. If the SCUBA-2 and HARP maps were subtracted in order to account for the molecular line contamination, there is a possibility that an overcompensation for the molecular line flux would occur, creating regions of negative flux in the dust continuum map.

An additional uncertainty in the contamination due to large-scale CO emission is the inclusion of the secondary beam in the calculation of the telescope beam area in equation (8), which increases the beam area by a factor of 1.2 at 850 μm (determined from a new FWHM calculated in Section 2.2). Large-scale emission couples to the telescope beam as the efficiency factor $\eta_{\rm fss}$ instead of $\eta_{\rm MB}$ (as in equation 11). Therefore, the conversion factor for ^{12}CO 3–2 would increase by a factor of 1.1, which is insignificant compared to other uncertainties. The scales of large-scale emission that could cause significant signal without being taken out by the S2SRO common-mode subtraction range from 13.8 arcsec (the FWHM of the 850 μm beam) to 1 armin (the Gaussian FWHM used in the GSM masking process). For the full SCUBA-2 array, CO emission on scales up to 8 arcmin in size could contribute.

CO is not the only possible contributor in the 850 and 450 μm bands. Studies of other molecular lines found SCUBA 850 μm line contamination from HCN, HNC, CN and methanol add together to form roughly 40 per cent of the total line contamination when observing other more energetic sources, like the shocked region SK1-OMC3 (Johnstone et al. 2003). Similar contamination was found in the Kleinmann–Low nebula, from SO and SO_2 emission that was 28–50 per cent of the total line contamination at 850 μm (Groesbeck, Phillips & Blake 1994; Serabyn & Weisstein 1995). Other studies have found the total line contamination by other molecular lines to be a factor of 2–3 times that from CO in outflows (Tothill et al. 2002; Gueth et al. 2003). Since molecular line contamination from other molecules is also likely, some features with low flux in the dust continuum may entirely be the result of line emission.

5.1 ^{12}CO 6–5 contamination

For the 450 μm band, we have no ^{12}CO 6–5 maps with which to estimate the CO contamination directly. Using the line intensities from the ^{12}CO 3–2 HARP maps, we can instead predict the potential line contamination from ^{12}CO 6–5 to the SCUBA-2 450 μm dust continuum signal.

Assuming local thermodynamic equilibrium, we can estimate the ratio of the main-beam brightness temperatures $T_{\rm MB}$ for ^{12}CO 6–5 and ^{12}CO 3–2. We assume that the excitation temperature, $T_{\rm ex}$, is equal to the kinetic temperature of the region, and is therefore the same for both ^{12}CO 3–2 and ^{12}CO 6–5. We also assume the partition function $Z \approx 2T_{\rm ex}/T_0$ and the Gaussian line shape $\theta(\text{peak}) = 2c\sqrt{2\ln 2}\,/\nu\,\Delta v\sqrt{2\pi}$, yielding the relation (in CGS

[5] http://star-www.rl.ac.uk/star/docs/sc19.htx/node40.html

units):

$$T_{\rm MB} = \frac{8\pi^3}{3h}\mu^2(J+1)^2\frac{T_0^2}{2T_{\rm ex}}\exp\left[\frac{-(J+1)(J+2)T_0}{2T_{\rm ex}}\right] \times\frac{2\sqrt{2\ln 2}}{\Delta v\sqrt{2\pi}}N_{\rm tot} \quad (13)$$

where h is Planck's constant, μ is the permanent electric dipole moment of the molecule, J is the lower rotational level of a linear molecule and T_0 is the ground-state temperature ($h\nu_0/k$) at 5.5 K. Using equation (13), the ratio ^{12}CO 6–5/^{12}CO 3–2 is as follows:

$$\frac{T_{\rm MB}(6\rightarrow 5)}{T_{\rm MB}(3\rightarrow 2)} = \frac{(6)^2}{(3)^2}\frac{\exp\left(\frac{-21\ T_0}{T_{\rm ex}}\right)}{\exp\left(\frac{-6\ T_0}{T_{\rm ex}}\right)} = 4\exp\left(-15\frac{T_0}{T_{\rm ex}}\right), \quad (14)$$

where $J(6\rightarrow 5) = 5$ for $T_{\rm MB}(6\rightarrow 5)$ and $J(3\rightarrow 2) = 2$ for $T_{\rm MB}(3\rightarrow 2)$.

Assuming that the source dust temperatures of 10 K, as in Section 4.2, are equal to the excitation temperature in the protostellar envelope, it follows from equation (14) that the ratio ^{12}CO 6–5/^{12}CO 3–2 is ∼0.001 in the optically thin case. The ratio between the two lines is low due to the low temperature of the region, indicating that there is less likelihood of detecting ^{12}CO 6–5 in cooler regions of the cloud. The sources analysed in NGC 1333, NGC 2071 and NGC 2024 with high ^{12}CO 3–2 contamination correspond to molecular clouds at temperatures of 20–25 K. At 25 K, the ratio of ^{12}CO 6–5/^{12}CO 3–2 is 0.147 in the optically thin case. However, outflows can contain even higher temperatures, ranging from 50 to 150 K (Hatchell, Fuller & Ladd 1999; van Kempen et al. 2009). At 50 K, the ratio is 0.769, indicating that ^{12}CO 6–5 is much more likely to be detected from outflows. If, on the other hand, both lines are optically thick, then the ratio tends to 1 as is known to be the case for ^{12}CO 3–2 (Buckle et al. 2010; Curtis et al. 2010).

Using the ratio ^{12}CO 6–5/^{12}CO 3–2, we can estimate typical peak fluxes for ^{12}CO 6–5: an excitation temperature of 25 K and a source with a typical ^{12}CO 3–2 integrated intensity of 100 K km s^{-1} will produce a corresponding ^{12}CO 6–5 flux contribution of 8 mJy beam^{-1} for Grade 2 weather in the 450 μm SCUBA-2 map. With the SCUBA-2 450 μm sensitivity for the Gould Belt Survey (Ward-Thompson et al. 2007) at an rms of ∼35 mJy beam^{-1} for Grade 2 weather, the ^{12}CO 6–5 flux contribution would not be detected. Even in the case of optically thick emission where the ratio ^{12}CO 6–5/^{12}CO 3–2 is 1, the ^{12}CO 6–5 is estimated to be 57 mJy beam^{-1}, which is under the 5σ detection limit.

Using published observations, ^{12}CO 6–5 contamination can be studied in further detail. ^{12}CO 6–5 data were taken for IRAS 2A, 4A and 4B in NGC 1333 by Yildiz et al. (2010). These sources are particularly bright and possibly intermediate-mass protostars. ^{12}CO 6–5 integrated intensities at the positions of the protostars were 57, 122 and 43 K km s^{-1}, respectively. Using the ^{12}CO 6–5 conversion factors calculated in this study for Grade 2 weather, the corresponding CO contamination to the SCUBA-2 450 μm dust continuum would be 32 mJy beam^{-1} (IRAS 2A), 70 mJy beam^{-1} (IRAS 4A) and 25 mJy beam^{-1} (IRAS 4B) for the CO contamination to the SCUBA-2 450 μm dust continuum. Peak fluxes from SCUBA were 2355, 7000 and 3025 mJy beam^{-1}, respectively (Hatchell et al. 2005). The SCUBA-2 450 μm dust emission peaks are a factor of several hundred times larger than the ^{12}CO 6–5 contribution. For these bright protostars, the CO contamination is insignificant at 450 μm.

Dust continuum fluxes in the 450 μm SCUBA-2 band are estimated to be a factor of 6 to 12 higher than fluxes in the 850 μm band. In the R–J approximation, the dust optical depth increases as $\lambda^{-\beta}$ with β between 1 and 2 and the corresponding flux density increases as λ^{-3} to λ^{-4} (Wilson 2009). The increase in continuum flux at 450 μm clearly outweighs the expected contribution from ^{12}CO 6–5. At most the ^{12}CO 6–5 integrated main-beam emission is the same as the ^{12}CO 3–2 emission assuming optically thick emission. This situation corresponds to a molecular line ratio of 1 and a contamination flux ratio of 0.84 (assuming Grade 2 weather). Since 450 μm continuum fluxes increase with respect to the 850 μm continuum, 450 μm continuum measurements would more likely be contaminated by strong molecular outflows instead of other means, i.e. nearby stars or ambient cloud emission. Nonetheless, potential contamination could occur in particularly low flux sources with nearby molecular outflows, such as the sources in NGC 2071 that were near to confirmed outflow candidates (see Section 4.3).

In the case of large-scale ^{12}CO 6–5 emission, it is also necessary to include the secondary beam in the calculation of the 450 μm telescope beam (equation 8). The total beam area for 450 μm increases by a factor of 2.0 (determined from an effective FWHM calculated in Section 2.2). Using equation (11) with the efficiency factor $\eta_{\rm fss}$, the ^{12}CO 6–5 conversion factor would increase by a factor of 1.7. The increase in the expected 450 μm dust continuum flux still exceeds any change in the ^{12}CO line conversion factors. Therefore, our conclusion that there is little CO contamination in the 450 μm maps, as discussed above, still holds.

6 CONCLUSIONS

In this study, the ^{12}CO line contamination factors for the 450 and 850 μm SCUBA-2 continuum bands were calculated under different atmospheric conditions (weather grades 1 to 5). These contamination factors were then applied to three different regions, NGC 1333, NGC 2071 and NGC 2024, in order to study the HARP ^{12}CO 3–2 flux contribution to the SCUBA-2 850 μm measurements using a list of sources for each region. Sources with high ^{12}CO contamination (greater than 20 per cent) were analysed in further detail to determine the cause of the contamination. The following can be concluded from this study.

(i) For the 850 μm SCUBA-2 filter profile, the ^{12}CO 3–2 contamination factors increase as the sky opacity τ_{225} increases. The contamination factors (mJy beam^{-1} per K km s^{-1}) of ^{12}CO to the 850 μm dust emission are by weather grade: (Grade 1) 0.63, (Grade 2) 0.68, (Grade 3) 0.70, (Grade 4) 0.74 and (Grade 5) 0.77.

(ii) For the 450 μm SCUBA-2 filter profile, the ^{12}CO 6–5 contamination factors decrease as the sky opacity τ_{225} increases due to the atmosphere transmission steeply declining at higher opacity grades. The contamination factors (mJy beam^{-1} per K km s^{-1}) of ^{12}CO to the 450 μm dust emission are by weather grade: (Grade 1) 0.64, (Grade 2) 0.57, (Grade 3) 0.51, (Grade 4) 0.41 and (Grade 5) 0.35.

(iii) The ^{12}CO 3–2 contribution to the 850 μm SCUBA-2 dust continuum is typically under 20 per cent for all of the regions studied. However, in regions of molecular outflows, the ^{12}CO can reach a flux contribution of ∼68 mJy beam^{-1} for the sources studied, dominating the dust continuum in sources with both high and low continuum flux densities (up to 500 mJy beam^{-1}) with a contribution up to 79 per cent contamination. Peak ^{12}CO fluxes in molecular outflows in the regions reached even higher levels, up to 154 mJy beam^{-1}.

There is strong evidence that ^{12}CO 3–2 contamination, while mostly minimal, is a major potential source of confusion that can be observed directly in the 850 μm dust continuum maps resembling protostellar cores or filamentary structure (as may be the case in NGC 1333, NGC 2071 and NGC 2024).

(iv) Even though we have no ^{12}CO 6–5 molecular line maps to study in further detail, in hot (50 K) regions, e.g. molecular outflows, the ratio of main-beam temperature $T_{\rm MB}$ for ^{12}CO 6–5/^{12}CO 3–2 is ∼0.769. However, CO contamination to the 450 μm source fluxes is not expected to be as much of an issue because of the expectation for the 450 μm dust emission to be a factor of 6–12 times brighter than the 850 μm fluxes.

ACKNOWLEDGMENTS

We would like to thank Antonio Chrysostomou and Simon Coudé for their helpful input for this paper. The JCMT is operated by the Joint Astronomy Centre (JAC) on behalf of the Science and Technology Facilities Council (STFC) of the United Kingdom, the National Research Council of Canada and the Netherlands Organisation for Scientific Research. This work made use of SIMBAD that is operated at CDS, Strasbourg, France. We acknowledge the data analysis facilities provided by the Starlink Project which is run by CCLRC on behalf of PPARC. In addition, the following Starlink package AUTOPHOTOM has been used. This research made use of APLPY, an open-source plotting package for PYTHON hosted at http://aplpy.github.com. ED acknowledges the support of a college studentship from the University of Exeter.

REFERENCES

Aguirre J. E. et al., 2011, ApJ, 192, 4
Andre P., Ward-Thompson D., Motte F., 1996, A&A, 314, 625
André P., Bouwman J., Belloche A., Hennebelle P., 2003, in Curry C. L., Fich M., eds, SFChem 2002: Chemistry as a Diagnostic of Star Formation. NRC Press, Ottawa, Canada, p. 127
Brown A. G. A., de Geus E. J., de Zeeuw P. T., 1994, A&A, 289, 101
Buckle J. V., Hills R. E., Smith H., Dent W. R. F., Bell G., 2009, MNRAS, 399, 1026
Buckle J. V., Curtis E. I., Roberts J. F., White G. J., Hatchell J., 2010, MNRAS, 401, 204
Curtis E. I., Richer J. S., Swift J. J., Williams J. P., 2010, MNRAS, 408, 1516
Davis C. J., Dent W. R. F., Matthews H. E., Coulson I. M., McCaughrean M. J., 2000, MNRAS, 318, 952
Di Francesco J., Johnstone D., Kirk H., MacKenzie T., Ledwosinska E., 2008, ApJS, 175, 277
Enoch M. L. et al., 2006, ApJ, 638, 293
Evans N. J., II, Rawlings J. M. C., Shirley Y. L., Mundy L. G., 2001, ApJ, 557, 193
Gordon M. A., 1995, A&A, 301, 853
Groesbeck T. D., Phillips T. G., Blake G. A., 1994, ApJS, 94, 147
Gueth F., Bachiller R., Tafalla M., 2003, A&A, 401, L5
Hatchell J., Dunham M. M., 2009, A&A, 502, 139
Hatchell J., Fuller G. A., Ladd E. F., 1999, A&A, 344, 687
Hatchell J., Richer J. S., Fuller G. A., Qualtrough C. J., Ladd E. F., Chandler C. J., 2005, A&A, 440, 151
Hatchell J., Fuller G. A., Richer J. S., Harries T. J., Ladd E. F., 2007a, A&A, 468, 1009
Hatchell J., Fuller G. A., Richer J. S., 2007b, A&A, 472, 187
Hildebrand R. H., 1983, Q. J. R. Astron. Soc., 24, 267
Holland W., Duncan W., Griffin M., 2002, in Stanimirovic S., Altschuler D., Goldsmith P., Salter C., eds, ASP Conf. Ser. Vol. 278, Single-Dish Radio Astronomy: Techniques and Applications. Astron. Soc. Pac., San Francisco, p. 463
Johnstone D., Bally J., 1999, ApJ, 510, L49
Johnstone D., Bally J., 2006, ApJ, 653, 383
Johnstone D., Wilson C. D., Moriarty-Schieven G., Joncas G., Smith G., Gregersen E., Fich M., 2000, ApJ, 545, 327
Johnstone D., Boonman A. M. S., van Dishoeck E. F., 2003, A&A, 412, 157
Kirk H., Johnstone D., Di Francesco J., 2006, ApJ, 646, 1009
Lada C. J., Alves J., Lada E. A., 1996, AJ, 111, 1964
Launhardt R., Mezger P. G., Haslam C. G. T., Kreysa E., Lemke R., Sievers A., Zylka R., 1996, A&A, 312, 569
Mitchell G. F., Johnstone D., Moriarty-Schieven G., Fich M., Tothill N. F. H., 2001, ApJ, 556, 215
Motte F., André P., Ward-Thompson D., Bontemps S., 2001, A&A, 372, L41
Nutter D., Ward-Thompson D., 2007, MNRAS, 374, 1413
Ossenkopf V., Henning T., 1994, A&A, 291, 943
Papadopoulos P. P., Allen M. L., 2000, ApJ, 537, 631
Reid M. A., Wilson C. D., 2005, ApJ, 625, 891
Richer J. S., Hills R. E., Padman R., Russell A. P. G., 1989, MNRAS, 241, 231
Seaquist E., Yao L., Dunne L., Cameron H., 2004, MNRAS, 349, 1428
Serabyn E., Weisstein E. W., 1995, ApJ, 451, 238
Shirley Y. L., Evans N. J., II, Rawlings J. M. C., 2002, ApJ, 575, 337
Tothill N. F. H., White G. J., Matthews H. E., McCutcheon W. H., McCaughrean M. J., Kenworthy M. A., 2002, ApJ, 580, 285
van Kempen T. A. et al., 2009, A&A, 507, 1425
Ward-Thompson D., Motte F., Andre P., 1999, MNRAS, 305, 143
Ward-Thompson D. et al., 2007, PASP, 119, 855
Wilking B. A., Meyer M. R., Greene T. P., Mikhail A., Carlson G., 2004, AJ, 127, 1131
Wilson T. L., 2009, preprint (arXiv e-prints)
Yildiz U. A. et al., 2010, A&A, 521, L40
Young C. H., Shirley Y. L., Evans N. J., II, Rawlings J. M. C., 2003, ApJS, 145, 111
Zhu M., Seaquist E. R., Kuno N., 2003, ApJ, 588, 243

APPENDIX A: MOLECULAR OUTFLOW SPECTRA CRITERIA

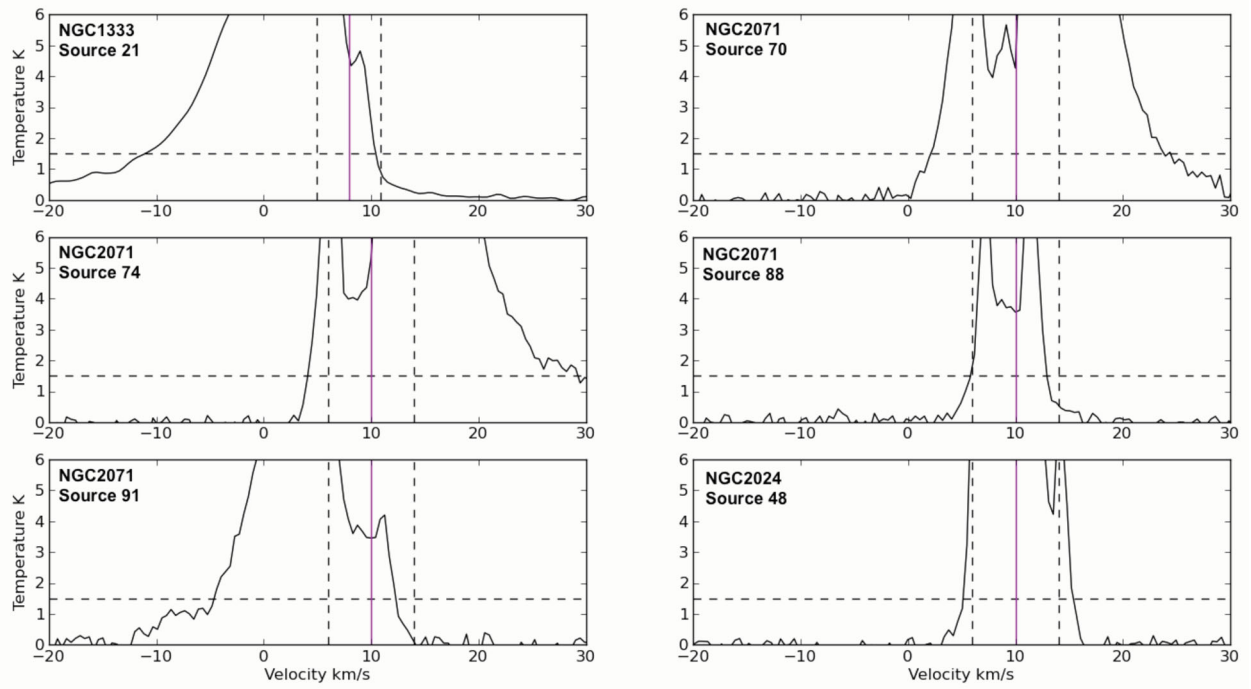

Figure A1. ^{12}CO 3–2 spectra for sources further analysed in Section 4.3 regarding the molecular outflow analysis. The core velocities are listed in Section 4.3.1 for NGC 1333 and in Table 3 for NGC 2071 and NGC 2024. Parameters $\pm 3\,\mathrm{km\,s^{-1}}$ for NGC 1333 and $\pm 4\,\mathrm{km\,s^{-1}}$ for NGC 2071 and NGC 2024 at 1.5 K were used to classify the presence of outflows.

This paper has been typeset from a TEX/LATEX file prepared by the author.